USGS
science for a changing world

Prepared in cooperation with the City of Prescott, the Town of Prescott Valley, and Salt River Project

Characterization of Big Chino Subbasin Hydrogeology near Paulden, Arizona, Using Controlled Source Audio-Frequency Magnetotelluric Surveys

Scientific Investigations Report 2019–5082

U.S. Department of the Interior
U.S. Geological Survey

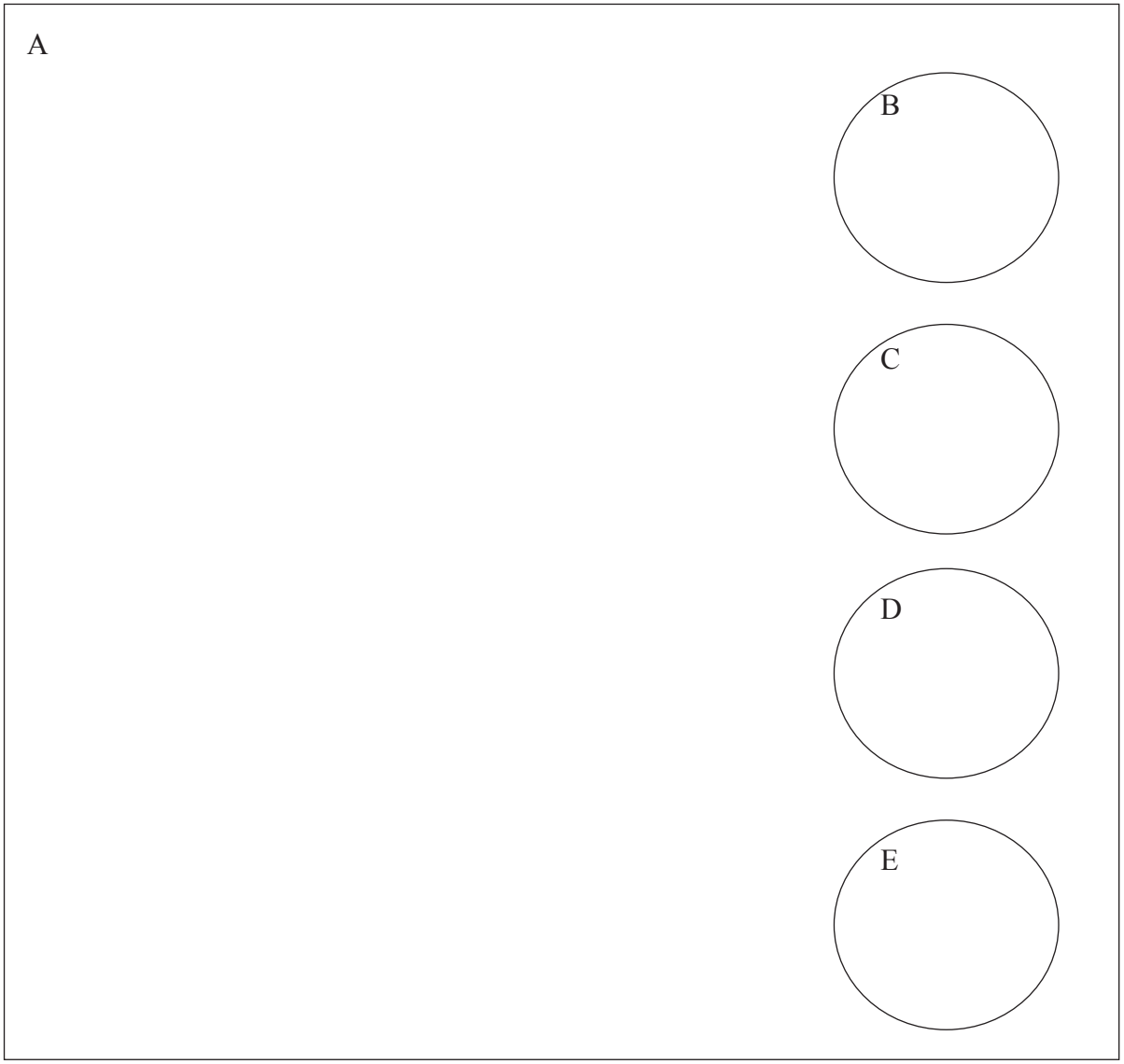

Cover. *A,* Outcrop of Devonian Martin Formation along south side of Verde River, just south of study area 1. *B,* Outcrop of fractured and jointed Tertiary basalt flow along Verde River, near south edge of study area 1. *C,* Outcrop of Precambrian crystalline and metasedimentary rocks in road cut along Williamson Valley Road, south of study area 2. *D,* Outcrop of Mississippian Redwall Limestone in road cut along Highway 89 where it cuts through the southeast end of Big Black Mesa, north of Paulden, Arizona. *E,* Outcrop of Quaternary fanglomerate in road cut along Highway 89, approximately 6 miles north of Paulden, Arizona. Photographs by Jon Mason, U.S. Geological Survey, 2019.

Characterization of Big Chino Subbasin Hydrogeology near Paulden, Arizona, Using Controlled Source Audio-Frequency Magnetotelluric Surveys

By Jamie P. Macy, Bruce Gungle, and Jon P. Mason

Prepared in cooperation with the City of Prescott, the Town of Prescott Valley, and Salt River Project

Scientific Investigations Report 2019–5082

U.S. Department of the Interior
U.S. Geological Survey

U.S. Department of the Interior
DAVID BERNHARDT, Secretary

U.S. Geological Survey
James F. Reilly II, Director

U.S. Geological Survey, Reston, Virginia: 2019

Suggested citation:
Macy, J.P., Gungle, B., and Mason, J.P., 2019, Characterization of Big Chino subbasin hydrogeology near Paulden, Arizona, using controlled source audio-frequency magnetotelluric surveys: U.S. Geological Survey Scientific Investigations Report 2019–5082, 39 p., https://doi.org/10.3133/sir20195082.

ISSN 2230-7102 (online)

Contents

Figures

Conversion Factors and Datums

Multiply	By	To obtain
	Length	
inch (in.)	2.54	centimeter (cm)
inch (in.)	25.4	millimeter (mm)
foot (ft)	0.3048	meter (m)
mile (mi)	1.609	kilometer (km)
	Area	
square mile (mi^2)	2.590	square kilometer (km^2)
	Volume	
acre-foot (acre-ft)	0.001233	cubic hectometer (hm^3)
	Flow rate	
cubic foot per second (ft^3/s)	0.02832	cubic meter per second (m^3/s)
gallon per minute (gal/min)	0.06309	liter per second (L/s)
gallon per year (gal/yr)	3.785	liter per year (L/yr)

Temperature in degrees Celsius (°C) may be converted to degrees Fahrenheit (°F) as follows:

°F=(1.8×°C)+32

Vertical coordinate information is referenced to the National Geodetic Vertical Datum of 1929 (NGVD 29). Altitude, as used in this report, refers to distance above the vertical datum.

Horizontal coordinate information is referenced to the North American Datum of 1927 (NAD 27).

Specific conductance is given in microsiemens per centimeter at 25 degrees Celsius (µS/cm at 25°C).

Concentrations of chemical constituents in water are given either in milligrams per liter (mg/L) or micrograms per liter (µg/L).

Characterization of Big Chino Subbasin Hydrogeology near Paulden, Arizona, Using Controlled Source Audio-Frequency Magnetotelluric Surveys

By Jamie P. Macy, Bruce Gungle, and Jon P. Mason

Abstract

The Big Chino subbasin is located in central-northwest Arizona in the transition zone between the Colorado Plateau and the Basin and Range Province. The controlled source audio-frequency magnetotelluric (CSAMT) geophysical method, a low-impact, non-intrusive, electrical resistance sounding technique, was used to evaluate the subsurface hydrogeology of the southern third of the Big Chino subbasin. The Big Chino subbasin is a northwest-trending, late Tertiary graben bordered by the Big Chino Fault along its northeast flank where there is as much as 1,100 meters of displacement. The main water-bearing stratigraphic unit of the basin is Tertiary alluvial-fill sediment. The Devonian Martin Formation provides water to wells near Drake and the Mississippian Redwall Limestone provides water to wells east of the basin and in the Paulden area.

The purpose of the CSAMT surveys was to improve the conceptual model of the aquifer by constraining the basin geometry and identifying stratigraphic units and their subsurface extents. CSAMT methods were used to map the subsurface along 100 kilometers (62 miles) of survey lines across the southern third of the subbasin. Of 21 survey lines, 14 were west of the town of Paulden and another 7 were east of Paulden. Data were cleaned and prepared for entry into Zonge SCS2D software and then inverted to provide a two-dimensional resistivity profile for each survey line. Final inversion models representing the best fit to measured data were compared to driller's logs or borehole data where present.

Data from the CSAMT lines west and north of Paulden are consistent with thicker alluvial basin deposits that range from 100 meters thick to a few hundred meters thick. Data from the CSAMT lines east of Paulden are consistent with thinner alluvial and basalt deposits overlying Paleozoic Martin Formation and Redwall Limestone, Tapeats Sandstone, and Precambrian granite and schist.

Introduction

The Big Chino Valley[1] of north-central Arizona (fig .1) was named by Amiel Weeks Whipple in 1853. He referred to it as "Val de Chino," claiming that "chino" was the local Mexican name for grama grasses (*Bouteloua* sp.), which grew throughout the valley (Barnes, 1988). Whipple described the grass of Val de Chino as "luxuriant." Even today no paved roads or major housing developments are found in most of the Big Chino Valley, and the grassland retains its ecosystem function as evidenced by the large population of free-ranging pronghorn antelope. The dominant activity in the Big Chino Valley today is ranching, and the grasslands remain among the most extensive and highest quality in the Verde River watershed (Graham, 2007), as they were when the Whipple expedition first arrived in 1853. Nonetheless, population growth across the adjacent 485-square-mile Prescott Active Management Area (PrAMA) remains high, having more than doubled from 1985 to 2005 (Rothman and Mays, 2014) with a continuing projected annual increase of about 2 to 3 percent per year (Collins and Bolin, 2007; Marder, 2009; Munoz-Erickson and others, 2010).

In recent years, Prescott (population 39,843 in 2010), Prescott Valley (population 38,822 in 2010), and Chino Valley (population 10,817 in 2010) (U.S. Census Bureau, 2018) have all had plans to pump from the Big Chino subbasin aquifer, as allowed by Arizona groundwater law, but as of 2018 no pumping has taken place. Downstream users of Verde River water, including Phoenix-area water provider Salt River Project, Cottonwood (population 11,265 in 2010), Camp Verde (population 10,873 in 2010), and Clarkdale (population 4,097 in 2010) (U.S. Census Bureau, 2018), and the Yavapai-Apache

[1] The Big Chino Valley is also referred to as the "Chino Valley" in the literature. In order to limit confusion with the nearby town of Chino Valley, "Big Chino Valley" will be used here.

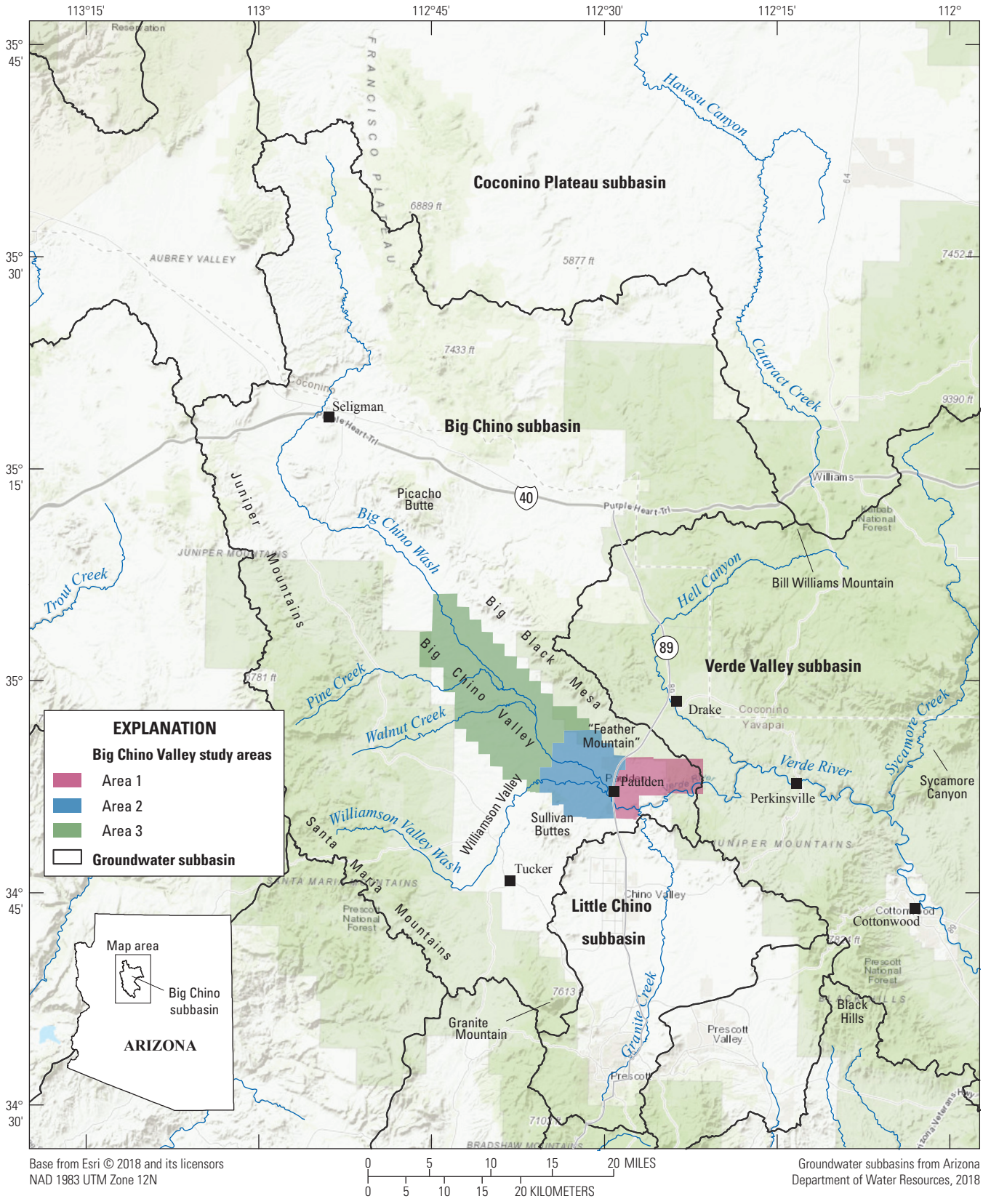

Figure 1. Location map of the Big Chino Subbasin showing the three areas of controlled-source audio-frequency magnetotelluric (CSAMT) surveys conducted in this study.

Nation (750 tribal members living in five tribal communities in Yavapai County in 2014; Yavapai-Apache Nation, 2018) are concerned that Big Chino subbasin groundwater withdrawals will eventually reduce the flow in the Verde River and water availability.

The upstream users' right to pump derives from the Arizona Groundwater Management Act (Arizona State Legislature, 1980). The Prescott Active Management Area (PrAMA) was designated in the Groundwater Management Act as one of four (now five) Active Management Areas in Arizona (Arizona State Legislature, 1980). In an active management area, withdrawal, transportation, and use of groundwater is regulated by the Groundwater Management Act. In addition, specific Active Management Areas may have additional regulations or authorizations that are unique.

In exchange for Central Arizona Project (CAP) water originally allocated to the PrAMA as well as a means to help settle local tribal water rights claims, certain government entities including the City of Prescott were authorized by a 1991 amendment to the Groundwater Management Act to annually pump and transport groundwater from the Big Chino subbasin into the PrAMA. The City of Prescott has statutory rights to pump up to 14,000 acre-feet of groundwater annually from the Big Chino subbasin. The Director of Arizona Department of Water Resources issued a final determination of this right in November 2009 that recognized 8,076.4 acre-feet as the total annual volume to which the City of Prescott is entitled (Arizona State Legislature, 1980; Arizona Department of Water Resources, 2014a,b,c). Additional groundwater of up to 3 feet per acre pumped from retired, historically irrigated acres is also legally available to municipalities in the PrAMA, although the total volume of such groundwater that a city or town can transport from the Big Chino subbasin has yet to be determined (Marder, 2009; Arizona Department of Water Resources, 2014b, 2014c; Arizona State Legislature, 1980).

The terminology used in this study follows Blasch and others (2006). In particular, "Big Chino subbasin" refers to the entire Big Chino drainage system including the valley floor and the bounding mountains where they drain into the Big Chino Wash. "Big Chino Valley" refers to the valley proper and only the immediately adjacent high-altitude areas. In addition, the structural basin is basically the floor of the Big Chino Valley, bounded by faults adjacent to Big Black Mesa to the northeast, primarily the Big Chino Fault, and a system of faults to the southwest along the Juniper Mountains and Williamson Valley. The geophysical surveys conducted for the current study took place on the Big Chino Valley floor, within the structural basin.

The Big Chino subbasin is 1,850 square miles (mi^2) and includes Big Chino Valley, Williamson Valley, and Walnut Creek (fig. 1; Blasch and others, 2006; Wirt and others, 2005; Arizona Department of Water Resources, 2014d). The Big Chino Valley is bounded by the Juniper and Santa Maria Mountains on the west side of the valley, the Granite Mountains on the south side, and Big Black Mesa and Bill Williams Mountain on the east side as well as the southern part of the Coconino Plateau to the north (Wirt and others, 2005; Blasch and others, 2006; Arizona Department of Water Resources, 2014d). Big Chino Valley is bisected from northwest to southeast by Big Chino Wash. The northwestern extent of the Big Chino subbasin is 13 miles (mi) north of Seligman and the southeastern extent is about 50 mi southeast of Paulden (fig. 1). The so-called "headwaters," a series of springs to the east of Paulden, is where the Verde River begins. Wirt and others (2005), Blasch and others (2006), and Pool and others (2011) all provide comprehensive summaries of previous studies of the Verde River watershed including the Big Chino subbasin, and the reader is referred there for research that provides additional hydrogeological context for the Big Chino subbasin.

This CSAMT study of the Big Chino subbasin better defines aquifer and lithologic extents (in particular sands and gravels versus silts and clays), which contribute to aquifer storage properties. The information provided here will improve the accuracy of distributions of hydraulic and storage properties in groundwater flow models of the Big Chino subbasin, which can then be used to estimate capture rates by groundwater withdrawals.

Purpose and Scope

This report describes a series of controlled-source audio-frequency magnetotelluric (CSAMT) electromagnetic profiles of the Big Chino subbasin that were obtained from surveys conducted from 2015 to 2017. By surveying the electrical properties of the subsurface using CSAMT techniques, geophysicists are able to infer stratigraphic and structural characteristics of the Big Chino subbasin, and thus improve understanding of the total hydrogeologic system. Twenty-one CSAMT surveys were conducted across the southern half of the Big Chino subbasin (fig. 2). The results of these surveys were used to improve the knowledge of lateral extent and depth of aquifer structure and the distribution of major aquitards (silt and clay layers and non-fractured volcanic intrusions) across the southern part of the Big Chino subbasin relative to major water-bearing intervals (sands and gravels), as well as the underlying extents of limestone aquifers and the non-aquifer crystalline rock. This information may be useful in future groundwater modeling efforts to better understand the timing and variations in groundwater discharge to the Verde River, in response to future variations in groundwater withdrawals and recharge.

Previous Investigations

Investigations directly relevant to the hydrology of the Big Chino Valley area include Wallace and Laney (1976), who produced water-level maps in the southern part of the Big Chino subbasin, including Williamson Valley, that were subsequently updated by Schwab (1995). The U.S. Geological Survey (USGS) conducted seepage investigations along the Verde River from near the mouth of Granite Creek to Camp Verde in June 1977 (U.S. Geological Survey, 1979; Owen-Joyce and Bell, 1983), and from Granite Creek to Sycamore Canyon in November 1999 and June 2000 (Wirt and others, 2005). As

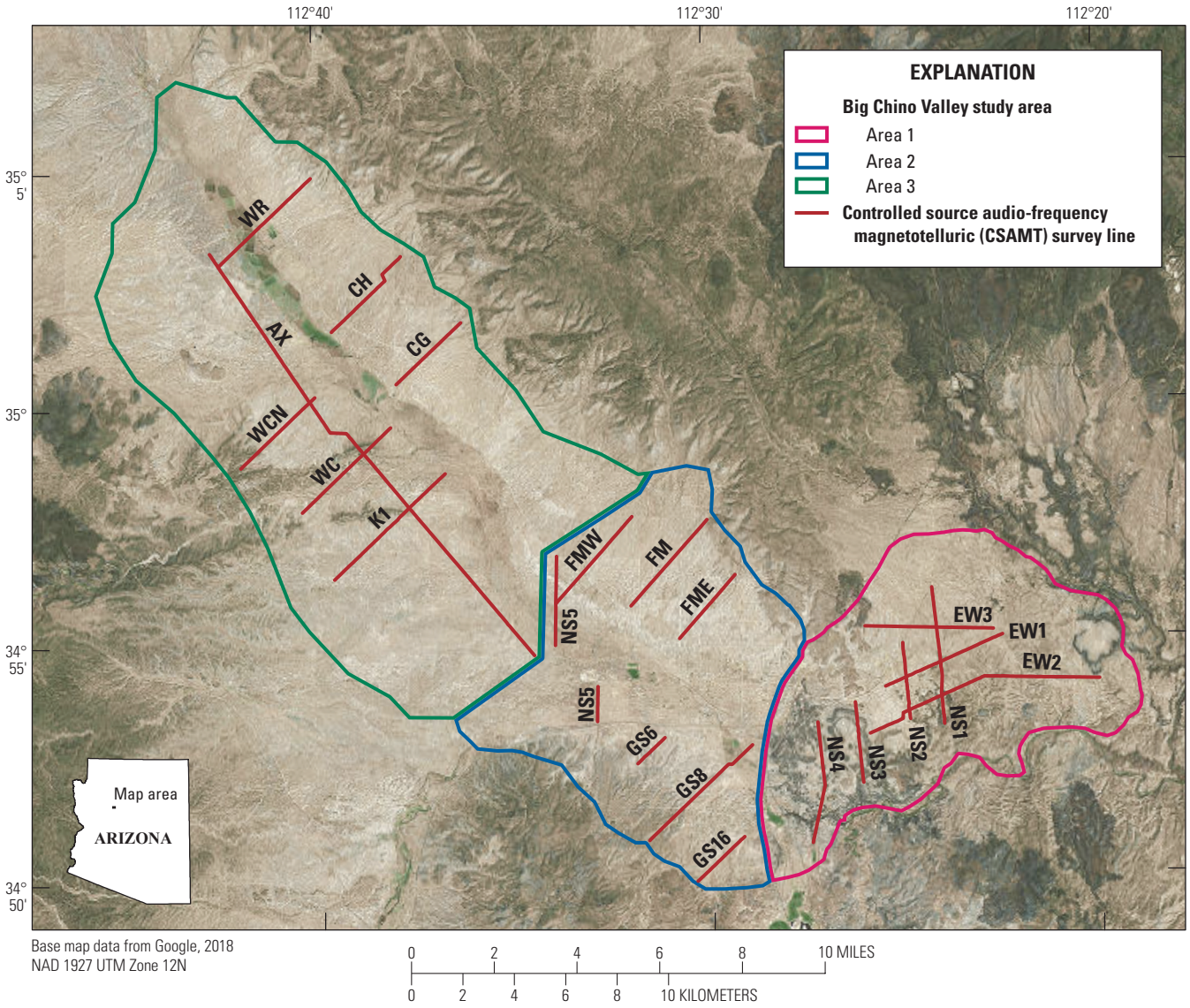

Figure 2. Map of the study area in the Big Chino subbasin showing the three individual areas of the controlled source audio-frequency megnetotelluric (CSAMT) surveys and the 21 CSAMT survey lines.

part of a hydrology and hydrogeologic study of Big Chino Valley, Ewing and others (1994b) conducted a seepage investigation in July 1991 from about half a mile above Granite Creek to Clarkdale. Other Verde River seepage investigations that begin at Clarkdale (for example, U.S. Geological Survey, 1980; Garner and Bills, 2012) and continue downstream are less relevant to the volume of groundwater discharging from the Big Chino subbasin.

Owen-Joyce and Bell (1983) described the geology, base flow, water chemistry and groundwater budget of the upper Verde River (parts of the upper and middle Verde River watersheds of Blasch and others, 2006), and provided a map of the hydrologic conditions. Freethey and Anderson (1986) included the Big Chino subbasin on one of their 72 maps that describe the predevelopment hydrologic conditions of southwest alluvial basins. Wilson (1991, sheet 1) compiled groundwater pumping in the Big Chino subbasin from 1950 to 1985. The Bureau of Reclamation conducted an extensive geologic framework investigation of the Big Chino Valley that included a wide range of geophysical techniques (Ostenaa and others, 1993; Ewing and others, 1994a) and an evaluation of groundwater and surface water supplies that included a seepage run in the uppermost Verde River (Ewing and others, 1994b). That study was undertaken with the City of Prescott in order to examine the relation between groundwater in the Big Chino subbasin and base flow in the Verde, and resulted in two calibrated, steady state models (Ewing and others, 1994b). Wirt and Hjalmarson (2000) evaluated the source of the upper Verde River springs that provide base flow to the Verde River from Granite Creek to Perkinsville; they determined the source to be mainly Big Chino subbasin groundwater. Navarro (2002) constructed a two-layer, three-aquifer groundwater flow model

of the Williamson Valley section of the Big Chino subbasin. Wirt and others (2005) described the geologic framework of the upper Verde River watershed based on a synthesis of the existing geologic, geophysical, hydrologic, and geochemical data. Blasch and others (2006) described the hydrogeologic framework, surface-water flow systems, and groundwater flow systems of the upper Verde River watershed including the Big Chino subbasin. Pool and others (2011) developed a three-layer numerical groundwater flow model of the primary aquifers of northern and central Arizona. This included the entire Big Chino subbasin.

Some geophysical work has previously been conducted in the Big Chino subbasin. Ostenaa and others (1993) of the Bureau of Reclamation conducted 21 resistivity soundings intended to delineate the extent of the clay and silt sediments of the Big Chino subbasin basin fill and to develop a general sense of the electrical properties and structure of the subbasin. Four profiles were generated from these soundings: one along the axis of the Big Chino Valley that extends about 20 kilometers (km) through our areas 2 and 3 (fig. 1), and the other three (about 6 to 15 km in length) perpendicular to the valley axis. Two of those profiles were in our area 2 and one in area 3 (fig. 1).

A seismic reflection survey was also conducted by Ostenaa and others (1993), and they delineate four stratigraphic horizons using this method, including the top of the Devonian Martin Formation, as well as a number of faults. In addition, they conducted borehole logging in 15 drill holes in the Big Chino subbasin to better characterize the lithologies in the region and to obtain quantitative values of resistivity and seismic velocity to assist with interpretation of the profiles obtained from the surface geophysical surveys.

Frank (1984), Water Resources Associates (1989), Dater and others (1999), and Langenheim and others (2000; 2002; 2005) all conducted bouguer gravity anomaly surveys in the Big Chino subbasin. Langenheim and others (2005) of the U.S. Geological Survey analyzed aeromagnetic survey data and gravity data to evaluate geologic structure in the upper Verde River watershed including the Big Chino and Little Chino subbasins. Volcanic centers down-gradient of springs, paleochannels subsequently filled with basalt, and a predominantly northeast- to north-striking structural grain in the Proterozoic basement rocks were among their many findings. They were also able to better characterize known fault systems and to identify previously unknown structural basins.

Physiography

The study area is located in the Transition Zone, the region between the Colorado Plateau and Basin and Range Province (fig. 3). Also sometimes referred to as the Central Highlands, the Transition Zone makes up about 15 percent of Arizona's total land area, but it is responsible for about 50 percent of the streamflow that originates in Arizona (Montgomery and Harshbarger, 1989). The Transition Zone contains topographic elements that were inherited from both the Colorado Plateau Province and the Basin and Range Province. Northwest-trending monoclines that were formed on the Colorado Plateau during the Laramide deformation are present in the Transition Zone, along with escarpments formed by normal faulting that occurred during Basin and Range extension. The Basin and Range extension was the last major stage of Transition Zone formation. It occurred in the Middle Tertiary, possibly in response to the subduction of a crustal spreading ridge and its associated mantle plume on the western plate margin of the North American continent (Dixon and Farrar, 1980). Subduction of the mantle plume is thought to have caused continental crust of the Basin and Range Province to stretch and thin by as much as 100 percent through a combination of high and low angle normal faulting (Spencer and Reynolds, 1989). The thinning of the Basin and Range continental crust lead to its subsidence in elevation relative to the Colorado Plateau, resulting in the final phase of Transition Zone formation. Normal faulting in the study area related to the Basin and Range extension deformed the bedrock into a northwest-trending graben structure that defines present-day Big Chino Valley (Blasch and others, 2006).

Base data from U.S. Geological Survey 60-meter digital data
Albers Equal-Area Conic projection, NAD 1983

Figure 3. Map of Arizona showing its physiography, notably the Transition Zone region between the Colorado Plateau and the Basin and Range Province. The location of the three parts of our study area are shown in the north-central part of the Transition Zone.

Geology

Rocks and sediments found in the study area are a product of the long and complex geologic history of the region. According to DeWitt and others (2008), some basement rocks in the study area are older than 1.7 billion years (Ga). The rocks and sediment present today in the study area do not, however, provide a complete timeline of geologic history. There are numerous gaps in the geologic record representing periods of either non-deposition or erosional events that removed earlier deposits.

Precambrian Formations

DeWitt and others (2005) reported that granite is found under much of Chino Valley and that from Sullivan Buttes to north of Paulden metasedimentary rocks are in contact with the granite. Large outcrops of Precambrian rocks occur several miles to the west of Big Chino Wash with smaller outcrops along Big Black Mesa and the Verde River (DeWitt and others 2008; figs. 4 and 5).

Blasch and others (2006) reported that in general, Precambrian rocks in the upper and middle Verde watersheds do not store enough water to be productive aquifers. An exception to this outside the study area is the fractured and weathered granite between the Little Chino subbasin and Williamson Valley, where hundreds of wells produce water from granite (Blasch and others, 2006). In the adjacent Little Chino and Agua Fria subbasins, Wilson (1988) and Corkhill and Mason (1995) concluded that the crystalline or foliated igneous and metamorphic basement rocks are generally dense, nonporous, and nearly impermeable (figs. 4 and 5).

Paleozoic Formations

DeWitt and others (2008) described the Tapeats Sandstone as reddish-brown sandstone and conglomerate ranging in thickness from 15 to 85 meters (m). Blasch and others (2006) reported that little is known about the water-bearing properties of the Tapeats Sandstone in the upper and middle Verde watersheds due to a lack of well data, but Wirt and others (2005) reported that low permeability in the Tapeats is due to its strong cementation. The Tapeats Sandstone outcrops near the study area along much of the southwest side of Big Black Mesa, in a band along the southern base of the Juniper Mountains near Walnut Creek, and in areas of the Santa Maria Mountains (DeWitt and others, 2008; figs. 4 and 5).

DeWitt and others (2008) described the Bright Angel Shale as gray shale and minor dolomite. The shale outcrops near the study area in a thin band along the south and east sides of the Juniper Mountains where Middleton and Elliot (2003) reported it to be only a few feet thick (figs. 4 and 5). The Bright Angel Shale is a confining unit and forms the effective base of the Big Chino aquifer system in places (Pool and others, 2011).

DeWitt and others (2008) described the Martin Formation as dark-gray dolomite, minor limestone, and sandy siltstone with a thickness of about 105 to 145 m. The Martin Formation is exposed along the Verde River in study area 1, just outside the study area along the southwest side of Big Black Mesa, and in a band around the Juniper Mountains (figs. 4 and 5). Wirt and others (2005) reported that the formation has moderate overall permeability with abundant northwest-striking high-angle joints near its base and locally includes solution cavities.

DeWitt and others (2008) described the Redwall Limestone as gray limestone with minor chert. They further stated that it has extensive karst development and collapse features, and a thickness ranging from 75 to 85 m. The limestone is exposed in a few locations within study area 1, and just outside of the study area on Big Black Mesa and in the Juniper Mountains (figs. 4 and 5). Wirt and others (2005) reported that the formation has high overall permeability.

The Schnebly Hill, Hermit, and Supai Formations were mapped as an undivided unit by DeWitt and others (2008) in an area adjacent to the Big Chino subbasin (figs. 4 and 5). In study area 1, the Supai Formation was mapped by DeWitt and others (2008) as its own unit, but for simplicity, we have combined these two map units into an undivided unit, PIPss, in figures 4 and 5. DeWitt and others (2008) described the undivided unit as a 330-m-thick section of sandstone, siltstone, and minor dolomite and conglomerate, and they map outcrops on the north side of Big Black Mesa, in the Juniper Mountains, and just to the south and southwest of Picacho Butte (fig. 4). These units are absent in the few available lithologic logs from wells that penetrate the late Paleozoic strata in Big Chino Valley.

The Kaibab Limestone and Coconino Sandstone of late Paleozoic age are presumed to be absent from the study area. There are no outcrops of these formations mapped in the study area and both units are missing from available lithologic well logs, although an outcrop of Coconino Sandstone was mapped by Dewitt and others (2008) on the south side of Picacho Butte outside of the study area (fig. 4). It is less clear whether late Paleozoic units below the Coconino Sandstone (Schnebly Hill, Hermit, and Supai Formations) are present in Big Chino Valley. These rocks are present in the higher terrain surrounding the valley, but absent in the few available lithologic logs from wells that penetrate the late Paleozoic strata in the valley. Cross sections of Big Chino Valley presented by Blasch and others (2006) and by Ostenaa and others (1993) do not include late Paleozoic formations.

Cenozoic Units

During the Tertiary, widespread volcanism occurred in the study region, mainly concentrated in two periods (Blasch and others 2006; DeWitt and others 2005). The first period of volcanism, during the middle Miocene prior to Basin and Range extension (Blasch and others, 2006; Coney and Reynolds, 1977; Spencer and Reynolds, 1989), was marked by the eruption of andesite and lati-andesite and the region was subsequently extended by low-angle faulting and rotation (Blasch and others, 2006). Wirt and others (2005) noted that "lati-andesite flows contain intersecting cooling fractures and

joints that give the lati-andesite a moderate overall permeability," but that "intrusive centers of lati-andesite have very low permeability." Blasch and others (2006) reported that where impermeable, lati-andesite can act as a barrier to groundwater flow. Outcrops of lati-andesite west of Big Chino Valley suggest continuity of the volcanic field across much of Williamson Valley Wash and some of southern Big Chino Wash. Near Big Chino Valley andesite or lati-andesite outcrops in the Sullivan Buttes volcanic field, along Walnut and Pine Creeks, and in the Juniper Mountains (DeWitt and others, 2005) (fig. 4).

The second period of volcanism occurred during and after Basin and Range extension and was dominated by alkaline basalts (Spencer and Reynolds, 1989; van Wijk and others, 2010; Sine and others, 2008). DeWitt and others (2005) reported that from about 66 to 4 Ma extensive basalt flows erupted along the Mogollon Rim and flowed into Big Chino Valley and the Verde River watershed east of Paulden. DeWitt and others (2005) further reported that sources of some of the flows were probably local cinder cones. Wirt and others (2005) reported that the columnar jointing that resulted from the cooling of these flows explains why the basalt has such high permeability. Basalt outcrops in much of area 1 and underlies younger sediments in a few well logs in areas 2 and 3 (DeWitt and others, 2008).

During the Tertiary, normal faulting around the study area related to Basin and Range extension resulted in the formation of Big Chino Valley. The topographic relief between the newly formed valley and surrounding uplands led to the deposition of a thick Tertiary sedimentary section in the valley. DeWitt and others (2008) mapped a Tertiary mixed sedimentary unit comprised of siltstone, sandstone, and minor conglomerate that extends into our area 3 from the west along Walnut Creek. This Tertiary sedimentary unit is derived from the Santa Maria Mountains to the southwest and in southern exposures contains thin basalt flows (DeWitt and others, 2008). Based on drilling and gravity data reported by Langenheim and others (2002), it appears this sedimentary unit thickens to as much as 800 m in Williamson Valley Wash near Tucker (DeWitt and others, 2008). Drill hole data indicate that Tertiary age sediments occur under much of the Quaternary deposits in Big Chino Valley (Dewitt and others, 2008).

DeWitt and others (2005) also described Tertiary playa deposits in Big Chino Valley. These deposits do not outcrop at the surface and are only known from well logs and drill cuttings. The extent of the deposits are not known, but DeWitt and others (2005) documented them in three drill holes separated by several miles. The thickness of the deposits varies from less than 30 m in a drill hole west of Big Chino Wash to about 500 m in a drill hole near the Big Chino Fault (DeWitt and others, 2005). The Arizona Department of Water Resources (2000) reports Tertiary basin fill as the major water-bearing unit in Big Chino and Williamson Valleys.

Quaternary Deposits

Quaternary deposits in the study area consist of alluvial fan deposits (fanglomerate), fine-grained alluvial sediments, terrace gravels, gravel, and recent stream alluvium. The original Quaternary map units of DeWitt and others (2008) have been simplified in figures 4 and 5 to combine units that are similar in composition. Blasch and others (2006) report that these units are typically highly permeable and locally yield water to shallow wells for domestic and agricultural purposes.

Structure

The structure of the study area is strongly related to the development of the Mogollon Rim at the southern edge of the Colorado Plateau and the normal faulting that created the Basin and Range Province farther south. The Mogollon Rim is a large escarpment that formed as a result of erosion and normal faulting (Elston and Young, 1991; Pierce and others, 1979). Elston and Young (1991) report that south of the Mogollon Rim, near-horizontal strata of lower parts of the Paleozoic section occur as erosional remnants. Some of these strata in the study area still have a northeasterly tilt inherited from the Colorado Plateau structure (DeWitt and others, 2005). Elston and Young (1991) concluded that the Transition Zone of central Arizona is a structural extension of the Colorado Plateau from which Paleozoic strata have been largely removed, exposing underlying Proterozoic basement. In addition, northwest-trending monoclines such as the Limestone Canyon monocline exposed on Big Black Mesa are reported by Davis (1978) to be the result of Laramide deformation of the Colorado Plateau.

Big Chino Valley is a "northwest-trending late Tertiary graben that is bordered on the northeast by the Big Chino Fault." The fault has at least 1,100 m of displacement in places and "decreases in displacement to the southeast and dies in a series of horsetail splays north of Paulden." (DeWitt and others, 2005). Wirt and others (2005) show that "displacement along the fault places basin deposits against granitic basement rock, creating a relatively impermeable boundary along most of Big Black Mesa, except where there is little displacement against Paleozoic carbonate rocks north of Paulden." Normal faults on the southwest side of Big Chino Valley are not as obvious and have less displacement, except north of Sullivan Buttes where several small faults are visible with various degrees of displacement (DeWitt and others, 2005). DeWitt and others (2005) conclude that "the Big Chino basin probably started to form at about 8–10 Ma. By 6 Ma, parts of the basin had a topographic form similar to its present-day shape" (fig. 4).

The boundary between study areas 1 and 2 is the approximate eastern boundary of the Big Chino Valley graben. The graben ends at a northeast-trending normal fault east of Highway 89. West of this fault, the Paleozoic formations are lower in elevation and buried under thick Cenozoic sediments and volcanic units. East of the fault, Paleozoic formations occur at the surface or below Tertiary volcanic rock (fig. 4). The Paleozoic formations in area 1 have a gentle northeasterly dip, probably related to Laramide deformation (DeWitt and others, 2005).

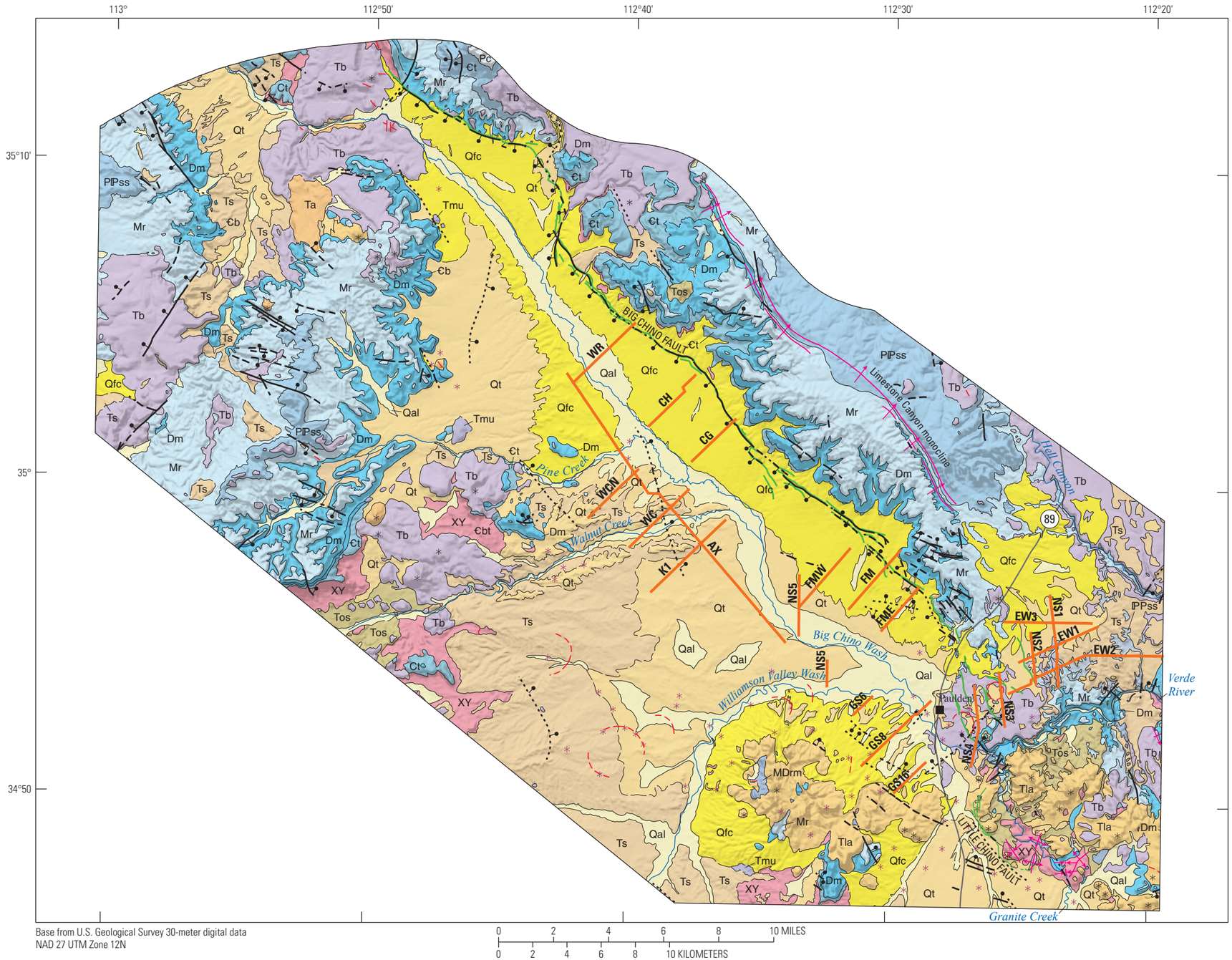

EXPLANATION

- Qal — Quaternary alluvium
- Qfc — Quaternary fanglomerates, colluvim, and sedimentary breccia
- Qt — Quaternary sediment, gravels, and terrace gravels
- Ta — Tertiary andesite
- Tb — Tertiary basalt
- Tla — Tertiary lati-andesite
- Tmu — Tertiary volcanic rocks
- Tos — Tertiary sedimentary rocks
- Ts — Tertiary sedimentary rocks and interbedded sedimentary and volcanic rocks
- Pc — Lower Permian Coconino Sandstone
- PIPss — Lower Permian and Upper Pennsylvanian Schnebly Hill, Hermit, and Supai Formations, undivided
- Mr — Mississippian Redwall Limestone
- Dm — Devonian Martin Formation
- MDrm — Mississippian Redwall Limestone and Devonian Martin Formation, undivided
- D€mt — Devonian Martin Formation and Cambrian Tapeats Sandstone of Tonto Group, undivided
- €b — Cambrian Bright Angel Shale of Tonto Group
- €t — Cambrian Tapeats Sandstone of Tonto Group
- €bt — Cambrian Bright Angel Shale and Tapeats Sandstone of Tonto Group, undivided
- XY — Precambrian crystalline and metasedimentary basement rock
- **Contact**—Dashed where approximately located
- **Fault**—Dashed where approximately located; dotted where concealed by younger units. Bar and ball on downthrown side where relative movement known
- Quaternary fault—Well constrained (U.S. Geological Survey and Arizona Geological Survey, 2018)
- Quaternary fault—Moderately constrained (U.S. Geological Survey and Arizona Geological Survey, 2018)
- **Anticline**
- **Monocline**
- **Syncline**
- **Dike**
- **Ring dike**—buried, location approximate
- EW2 — **CSAMT survey lines**
- **Volcanic center**
- **Buried volcanic center**

Figure 4. Geologic map of study area simplified from DeWitt and others (2008) with the controlled-source audio-frequency magnetotelluric (CSAMT) survey lines collected as part of this study.

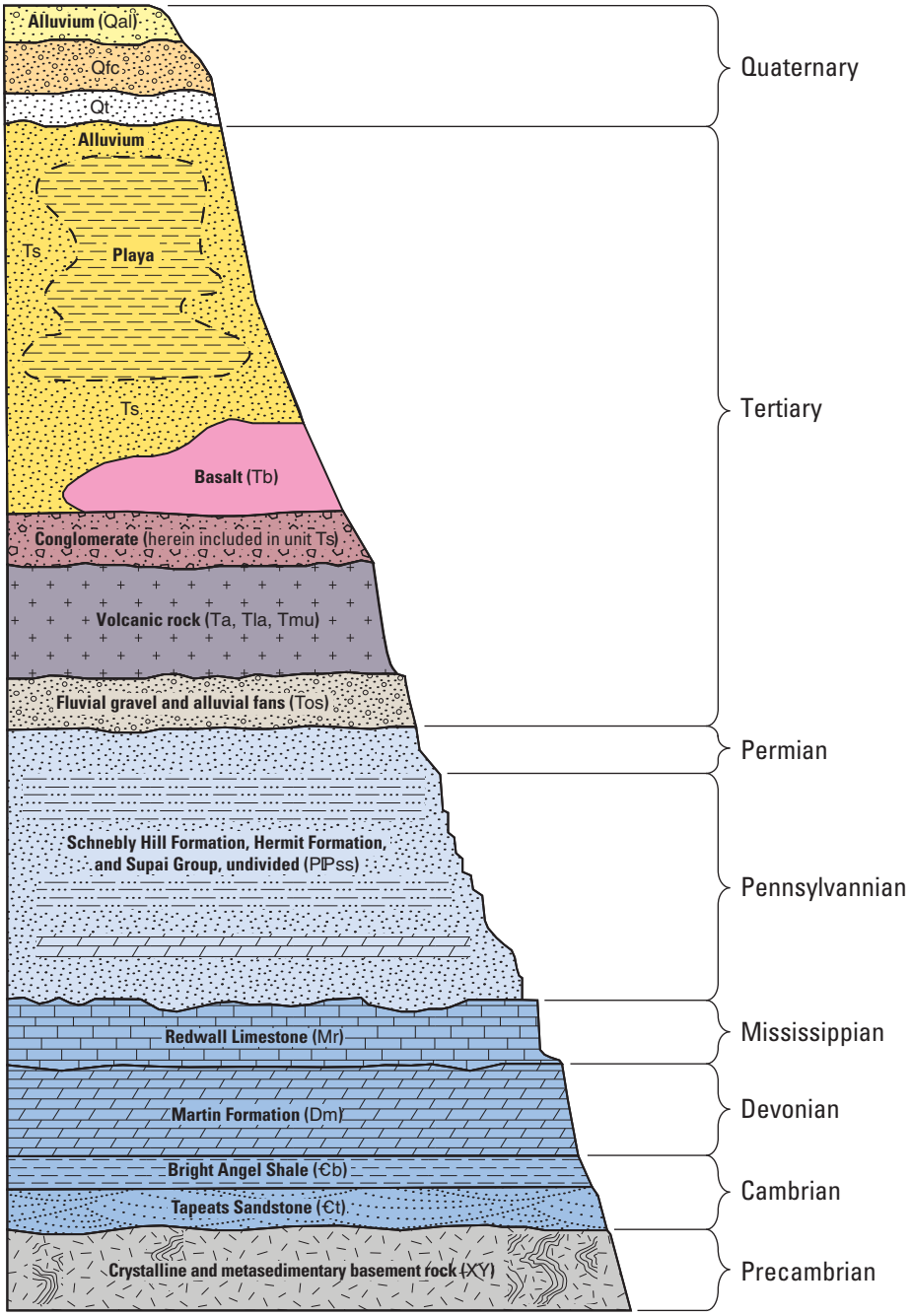

Figure 5. Generalized stratigraphic section for the Big Chino Valley study area, central Arizona (modified from Blasch and others, 2006, fig. 17). Map units modified from DeWitt and others (2008). Hermit, Supai, and Schnebly Hill Formations are present in the highlands surrounding Big Chino Valley, but it is uncertain if they are present in the valley itself.

Methods

This study uses surface geophysical surveys to develop a better understanding of the extent and lithologies of the Big Chino basin fill and carbonate aquifers. The method best suited to this study is controlled source audio-frequency magnetotellurics (CSAMT) because of the relatively fast data acquisition, ability to survey large areas, and ability to identify faults and stratigraphic units. Existing well logs and geophysical logs, water-level data, and other hydrogeologic information were used to constrain the subsurface electrical models.

Controlled Source Audio-Frequency Magnetotelluric Survey (CSAMT)

CSAMT is an electromagnetic sounding technique that has proven useful for hydrogeological and groundwater studies (Zonge, 1992). CSAMT is a low-impact, nonintrusive technique that has been used extensively by the minerals, geothermal, hydrocarbon, and groundwater exploration industries since 1978 when CSAMT equipment systems first became commercially available (Zonge, 1992). CSAMT can provide electrical resistivity information from the near-subsurface to

depths of about 3,000 m (about 9,800 ft) below land surface. Resistivity is a measure of a material's opposition to the flow of electrical current and typically is measured in ohm-meters (ohm-m). Because the electrical resistivity varies with rock types and water content, this method may provide an indication of subsurface structure (strata, faults, and fractures) and presence of groundwater (Simpson and Bahr, 2005). The higher the porosity of a rock, the lower the resistivity, and the higher the salinity of the saturating fluid, the lower the resistivity of the rock. Resistivity values for common near-surface earth materials vary by orders of magnitude, typically from 1 ohm-m or less for clays or alluvium saturated with high salinity water to 1,000 ohm-m or more for dry carbonates or crystalline rocks (Palacky, 1987). The resistivity of a rock is also dependent on saturation, porosity, fracturing, conductivity of fluids within the rock, and mineral composition (Zohdy and others, 1974). Saturated rocks have lower resistivity than unsaturated and dry rocks. Resistivity of sedimentary rocks, such as carbonates, typically ranges from 100 ohm-m to 2,000 ohm-m, while shales or claystones usually range from 1 ohm-m to 100 ohm-m, and sandstones can range from 20 ohm-m to 1,000 ohm-m. Igneous rocks, such as basalts, can range from 200 ohm-m to 1,000 ohm-m (Sumner, 1976: Nabighian and Macnae, 1987; Yungul, 1996).

Description of Method

CSAMT provides information on the electrical resistivity of the subsurface along a receiver profile by measuring electric and magnetic fields that are transmitted from a controlled current at several frequencies a specified distance away (fig. 6). Grounded dipoles at the receiver site detect the electric field parallel to the transmitter, and a magnetic-coil antenna senses the magnetic field perpendicular to the transmitter (fig. 6). The ratio of the orthogonal- and horizontal-electric field magnitudes to magnetic-field magnitudes yields the apparent resistivity, which is the true resistivity if the subsurface were homogeneous and isotropic. CSAMT uses a remote, grounded electric-dipole transmitter as an artificial signal source. The transmitter source provides a stable signal, resulting in higher precision and faster measurements than what can be obtained from natural source audio-frequency magnetotellurics. Typically, the source for a CSAMT survey is separated from the survey line by about a distance greater than three times the depth of investigation. For this study the depth of investigation was 300 to 500 m (fig. 6) (Zonge, 1992).

CSAMT measurements typically are made at frequency ranges from about 1 to 8,000 Hertz in binary incremental steps. The frequencies used for the surveys in this report were 2, 4, 8, 16, 32, 64, 128, 256, 512, 1,024, 2,048, 4,096, and 8,192 Hertz. CSAMT measurements consist of orthogonal and parallel components of the electric (E) and magnetic (H) fields at a separation of 4 to 10 km (3.1 to 9.3 mi) from the source (Sharma, 1997). CSAMT measurements can be taken in a number of different arrays depending on the type of information desired. This study used what is termed a "reconnaissance" type of CSAMT array, which consists of one electric (E_x) and one magnetic (H_y) component for each measurement (Zonge, 1992), as opposed to a more involved survey, which collects vector and tensor measurements by measuring two electric-field components (E_x and E_y) and three magnetic-field components (H_x, H_y, and H_z). Multiple electric fields are measured concurrently during reconnaissance CSAMT surveys. This study used a six-channel receiver, with the capability of simultaneously measuring five electric fields for every one magnetic field. Because the magnetic field does not change much over the same distance that substantial electric-field changes occur, fewer magnetic-field measurements are required. The magnetic-field measurement is used to normalize the electric fields and calculate the apparent resistivity and phase difference (Zonge, 1992). Grounded dipoles at the receiver site measure the electric field parallel to the transmitter (E_x), and a magnetic coil antenna measures the

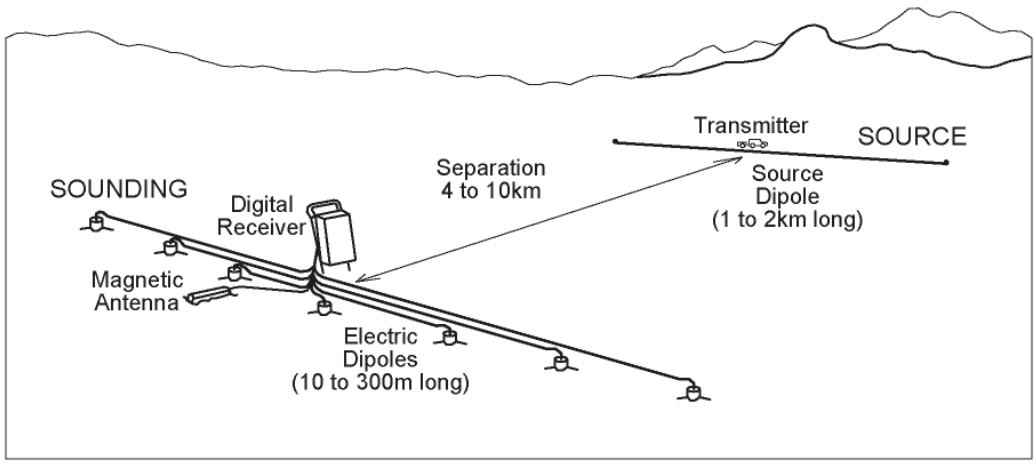

Figure 6. Cartoon showing the layout of a controlled source audio-frequency magnetotelluric survey (modified from Zonge, 1992).

perpendicular magnetic field (H_y). The ratio of the E_x and H_y magnitudes yields the apparent resistivity (eq. 1; Zonge, 1992; Simpson and Bahr, 2005):

$$\rho_a = \frac{1}{5} f \left[\frac{E_x}{H_y} \right]^2 , \quad (1)$$

where

ρ_a is the apparent resistivity in ohm-meters,

f is the frequency in Hertz,

E_x is the parallel electrical-field strength, and

H_y is the perpendicular magnetic-field strength.

The penetration of CSAMT into the subsurface and the depth of investigation are determined by the skin depth (eq. 2):

$$S = 503 \sqrt{\frac{\rho_a}{f}} , \quad (2)$$

where

S is the skin depth in meters,

ρ_a is the measured apparent ground resistivity in ohm-meters, and

f is the signal frequency in Hertz (Zonge, 1992; Simpson and Bahr, 2005).

The skin depth is the depth at which the amplitude of a plane wave signal has dropped to 37 percent of its value at the surface (Zonge, 1992). The skin depth is pertinent because CSAMT data are most commonly interpreted using simplified magnetotelluric (MT) equations based on the assumption that the electric and magnetic fields can be approximated as plane waves.

Unlike natural-source MT soundings, where the source of telluric current (distant lightning strikes or atmospheric interaction with solar winds) is considered infinitely distant and nonpolarized, the CSAMT source is finite in distance and distinctly polarized (Sharma, 1997). The separation, r, between the transmitter and receiver for CSAMT surveys must be greater than three skin depths for the current driven into the ground to behave like plane waves (termed "far field"). When r is less than three skin depths at the frequency being measured, the electric and magnetic fields no longer behave as plane waves and become curved (termed "near field") such that the equation for apparent resistivity (eq. 1) no longer applies. All data from this study used for modeling are measured in the far field. The minimum distance between the source and receiver was 5 km (3.1 mi), yielding an r of greater than three skin depths (Zonge, 1992).

When the r between the receiver and transmitter is greater than three skin depths, the equation for depth of investigation is (eq. 3; Zonge, 1992):

$$D = 356 \sqrt{\frac{\rho_a}{f}} , \quad (3)$$

The depth of investigation (D) of a CSAMT survey can range from 20 to 3,000 m (66 to 9,800 ft), depending on the resistivity of the ground and the frequency of the signal. Lower frequency signals have a greater depth of investigation than higher frequency signals. Equations 2 and 3 are used as a guideline or estimate for determining r and D, rather than a firm rule. During data analysis plotting of the apparent resistivity versus the frequency for a given set of soundings was used to determine the lowest far-field frequency.

Data Collection and Analysis

CSAMT data were collected in the Big Chino subbasin in Yavapai County, Arizona, from April 2015 to August 2017. A Zonge GGT-30 geophysical transmitter powered by and connected to a 25-kilowatt trailer-mounted generator and a Zonge XMT-32 transmitter controller were used to transmit the electrical source through a 1-kilometer-long (0.62 mi) dipole. A Zonge GDP-32II multichannel geophysical receiver was connected to six porous pot electrodes, which were filled with copper-sulfate solution and arranged in 100-m (328-ft) dipoles. A Zonge ANT6 high-gain mu-metal core magnetic antenna was used to measure the Earth's response to the transmitted signal. Each CSAMT field measurement consisted of one magnetic-field measurement (H_y) and five accompanying electric-field measurements (E_x).

CSAMT data can be influenced by nearby metal conductors such as fences, pipes, underground wires, overhead or buried power lines, and train tracks. Cultural interferences such as these were noted in the Big Chino subbasin and avoided when possible. Notch filters for 60, 180, 300, and 540 Hertz were used for all Big Chino subbasin CSAMT surveys to reduce noise.

Twenty-one CSAMT lines were surveyed as a part of this project—we assigned the designations AX, CG, CH, EW1, EW2, EW3, FM, FME, FMW, GS6, GS8, GS16, K1, NS1, NS2, NS3, NS4, NS5, WC, WCN, and WR (fig. 2)—for a total of 100 km (62 mi) of survey in the Big Chino subbasin in three geographic areas. Fourteen (66 km; 41mi) of the CSAMT survey lines were located west of the town of Paulden and seven (34 km; 21 mi) survey lines were located east of Paulden. The separation between transmitter and receiver locations ranged from about 5 km to 15 km (3 to 9 mi). Global positioning system (GPS) locations were marked for each receiver station using a Garmin 62st handheld GPS unit.

Once the surveys were complete, data were processed and analyzed using Zonge Engineering's DATPRO suite of software (Zonge Engineering, Tucson, Ariz.). Raw CSAMT data were first averaged using Zonge's CSAVG program. Averaged data were reviewed for near-field and far-field effects by plotting the apparent resistivity versus the frequency (eq. 2) for a given set of soundings. The lowest far-field frequency was determined based on these plots, and data below that frequency were not used in the analysis. Typically for the surveys in the Big Chino subbasin, 32 Hertz was the lowest

far-field frequency used for analysis. After determining the lowest far-field frequency, 32 to 8,192 Hertz data were averaged and entered into Zonge's SCS2D software for inversions. Topography and station locations were added to SCS2D using a station file. A two-dimensional finite-element algorithm is used by the modeling software, and the finite-element mesh is draped over an along-line topographic profile. The averaged data were inverted by Zonge's SCS2D software to provide a two-dimensional resistivity profile for each survey line. The profiles were then examined for errors and adjusted as appropriate. Additional adjustments were made to the inversion models in areas where the subsurface geology was known from lithologic logs of wells. For inversion purposes an assumed one-dimensional "layer-cake" resistivity structure is valid. Final inversion models presented in the "Results" section of this report represent the best fit to subsurface resistivity. Data to support the conclusions of this report are available from Macy and others (2018) on ScienceBase.

Results

The resistivity data collected along 21 CSAMT survey lines were inverted and modeled to display as cross sections. A total of 100 kilometers of linear survey lines were inverted into resistivity profiles and are discussed in three geographic areas: area 1 east of Paulden, area 2 west of but near the housing development in Paulden, and area 3 west of Paulden (fig. 2). CSAMT results in the Big Chino subbasin indicate a more electrically conductive subsurface west of Paulden, suggesting a deeper alluvial basin. East of Paulden, the surveys mapped extents and thicknesses of shallow alluvial and basalt cover over Paleozoic rocks, tops of crystalline rocks, and important geologic structures such as the Big Chino Fault. For interpretations on all geophysical plots, the label "fault" refers to a fault identified on a geologic map, and "potential fault" refers to an area where a fault has not been previously mapped but could be located based on information from the geophysical plot. Lithologic logs from selected wells and water levels were also included on the interpretations of the geophysical plots. A well was only included on the geophysical profile if it was used for driller's log information. Water levels were added to interpretations of the geophysical profiles if a water level was available from the general area of the geophysical profile.

Area 1

CSAMT lines NS1, NS2, NS3, NS4, EW1, EW2, and EW3 were completed in area 1 (fig. 2). Lines NS1 to NS4 are a series of lines oriented north to south and lines EW1 to EW3 are oriented east to west. Overall, area 1 has complex geology that includes layers of Quaternary and Tertiary alluvium and basalt, and Paleozoic Supai Formation, Redwall Limestone, Martin Formation, Tapeats Sandstone, and crystalline basement rocks (DeWitt and others, 2005; Blasch and others, 2006). The electrical properties of basalt and limestone can be difficult to differentiate because they are both electrically resistive, especially when the limestone occurs as a thin layer at the surface. Line NS1 is consistent with layered alluvium and Paleozoic sedimentary rocks overlying Precambrian rocks (fig. 7). At the northern end of line NS1, well MW-4b2 (B-18-01 19ADC) is located near station -225 (fig. 7). The lithologic log from the well shows that there is interfingering alluvium and basalt in the upper 35 m and the inverted resistivity section also supports this interpretation of the shallow subsurface along line NS1. On the resistivity plot of line NS1, the upper 35 m is material that's 100 ohm-m or less (green to yellow)(fig. 7). Below the upper layer is a much more resistive layer, typically 250 ohm-m (orange), that is consistent with Paleozoic Redwall Limestone and Martin Formation (fig. 7). There is a 700 m section of line between stations 1225 and 1925 that was skipped because of potential interference from power lines (fig. 7). Conductive material found at depth in this area is likely an artifact of the inversion due to lack of station data. To the south of station 1925, from elevation 1,165 to 1,200 m, the upper layer is alluvium and basalt, and there is a resistor or bedrock high below 1,165 m elevation that is stronger and more shallow than this line in the north (fig. 7). Line NS2 is
similar to line NS1 and has a thin, less than 50 m thick, 100 ohm-m or less (green to yellow) layer at the surface, which is consistent with alluvium and basalt (fig. 8). Below that is a much more resistive layer, 250 ohm-m or greater, consistent with Paleozoic Redwall Limestone and Martin Formation (orange to red)(fig. 8). There are gaps in line NS2 between stations 975 and 1325, and stations 1775 and 2225 because those areas were skipped due to power line interference (fig. 8). Conductive material found at depth in this area is likely an artifact of the inversion due to lack of station data and has been blanked out for the interpretation. South of station 1325 on line NS2 there is a bedrock high, below an elevation of 1,150 m, similar to line NS1 (figs. 7 and 8). Although there are no mapped faults at the surface, there appears to be a fault in the subsurface south of station 1925 on line NS1 and south of station 1325 on line NS2: the crystalline basement rock shallows by more than 100 meters almost instantaneously in this area (figs. 7 and 8). Both NS1 and NS2 show large resistivity increases to the north and those could be attributed to dry Paleozoic limestone.

The inverted resistivity sections from lines NS3 and NS4 show four lithologic layers (figs. 9 and 10). The upper most layer is moderately resistive, about 100 ohm-m or less (green to yellow), and extends from the surface to less than 50 m below land surface or 1,310 m elevation (figs. 9 and 10). This uppermost layer could be alluvium and (or) basalt. The second layer is a resistor, greater than 250 ohm-m (orange to red), from about 1,375 m to 1,275m elevation on NS3 (fig. 9), and 1,310 m to 1,200 m elevation on NS4 (fig. 10). This is interpreted to be the Paleozoic Redwall Limestone and Martin Formation. From 1,275 m to 1,200 m elevation on NS3 (fig. 9), and from 1,200 m to about 1,150 m elevation on NS4 (fig.10), there's a more conductive layer, less than 40 ohm-m (purple to green), that is consistent with the Tapeats Sandstone. A strong resistor, greater than 250 ohm-m (orange to red), is in the subsurface below an elevation of about 1,150 m on both lines, which is likely granite and schist bedrock (figs. 9 and 10). There is a gap in line NS4 from station 2950

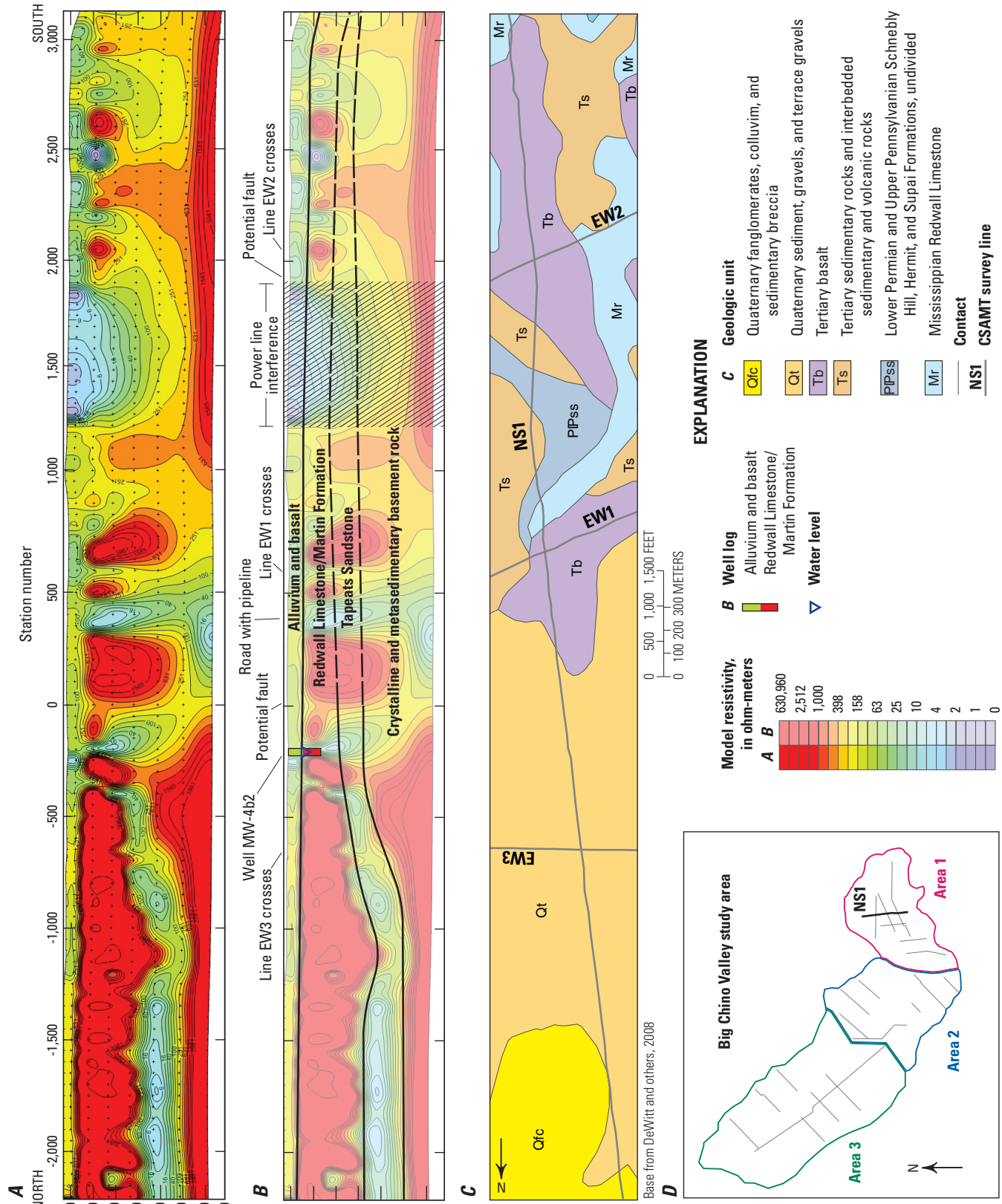

Figure 7. North to south cross section of controlled source audio-frequency magnetotelluric (CSAMT) smooth model inversion results for line NS1 (*A*). *B*, Interpretations of inversion results for line NS1. Diagonal line pattern denotes area of power line interference. *C*, Geologic map of area surrounding line NS1 (simplified from DeWitt and others, 2008). *D*, Location map of survey line NS1 and CSAMT profile, with line NS1 in black.

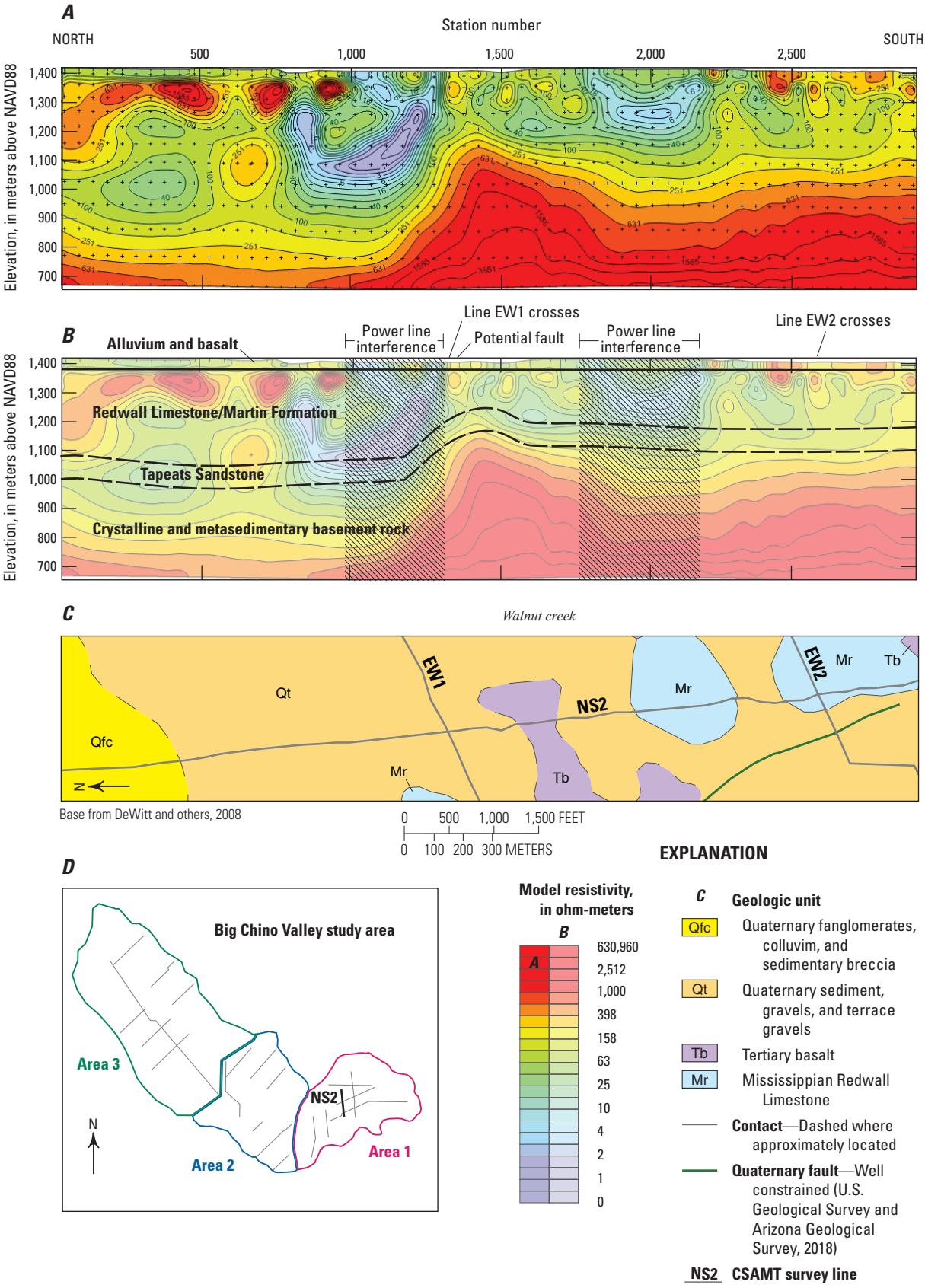

Figure 8. North to south cross section of controlled source audio-frequency magnetotelluric (CSAMT) smooth model inversion results for line NS2 (*A*). *B*, Interpretations of inversion results for line NS2. Diagonal line pattern denotes areas of power line interference. *C*, Geologic map of area surrounding line NS2 (simplified from DeWitt and others, 2008). D, Location map showing survey line NS2 and CSAMT profile, with NS2 in black.

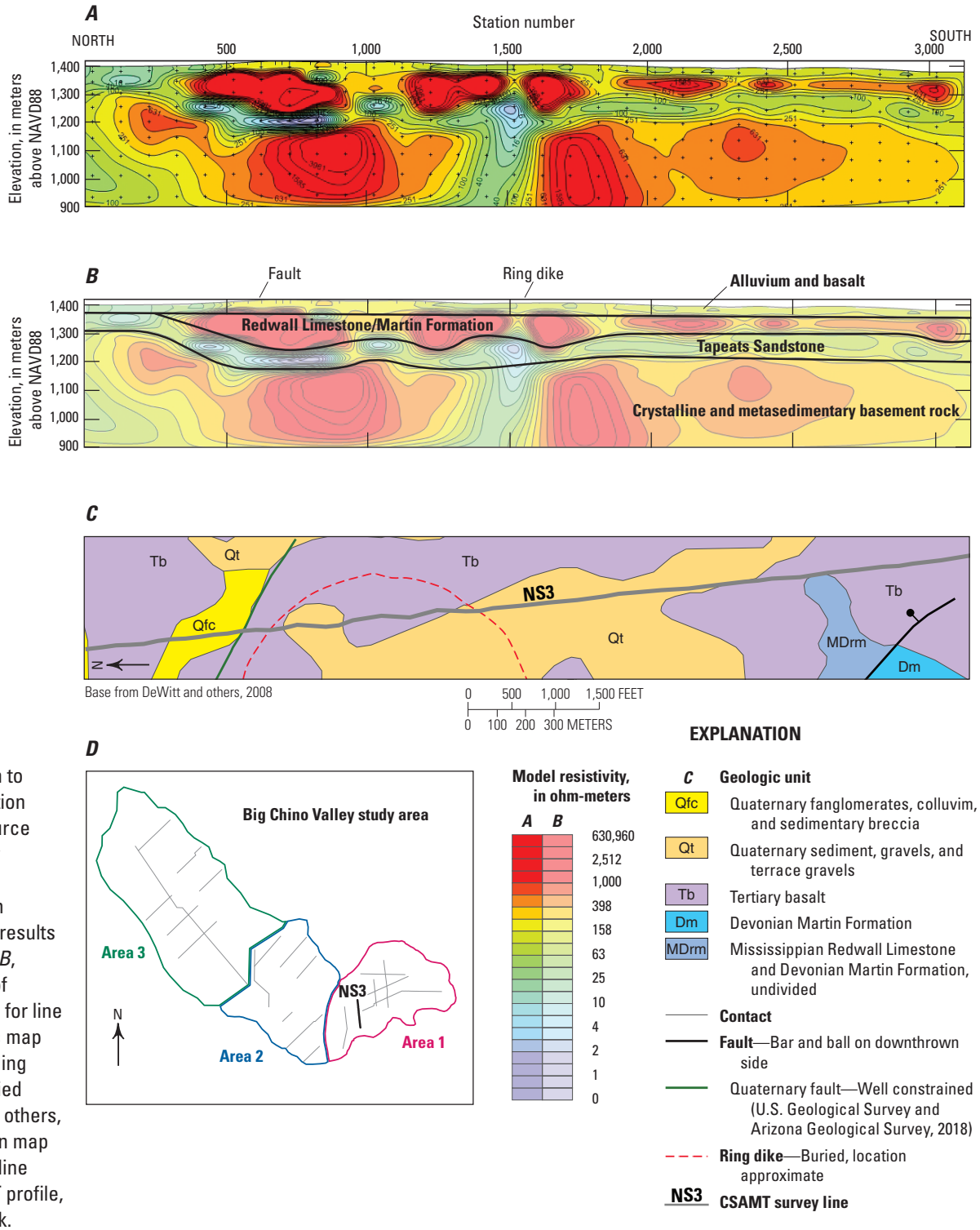

Figure 9. North to south cross section of controlled source audio-frequency magnetotelluric (CSAMT) smooth model inversion results for line NS3 (*A*). *B*, Interpretations of inversion results for line NS3. *C*, Geologic map of area surrounding line NS3 (simplified from DeWitt and others, 2008). *D*, Location map showing survey line NS3 and CSAMT profile, with NS3 in black.

to 4050, which is the area of the Verde River (fig. 10). The geology north and south of the Verde River along line NS4 is different; the large resistor below 1,150 m north of the Verde River is found at an elevation of about 1,250 south of the Verde River (figs. 10). This change along the river corridor suggests that there is a subsurface fault somewhere in the area of the Verde River that uplifts the granite and schist basement rock north of the Verde by about 100 to 150 m relative to the south side of the river.

Lines EW1 to EW3 are similar to the NS lines in that they show four distinct lithologic layers. The uppermost layer extends from the surface to less than 50 m below land surface or about 1,320 m elevation and is moderately resistive, about 100 ohm-m or less (green to yellow) (figs. 11–13). This uppermost layer could be alluvium and (or) basalt, and in the case of EW2 it's Supai Formation because it's mapped at the surface. The second layer is a resistor, greater than 250 ohm-m (orange to red), from about 1,320 m elevation to 1,220 m elevation

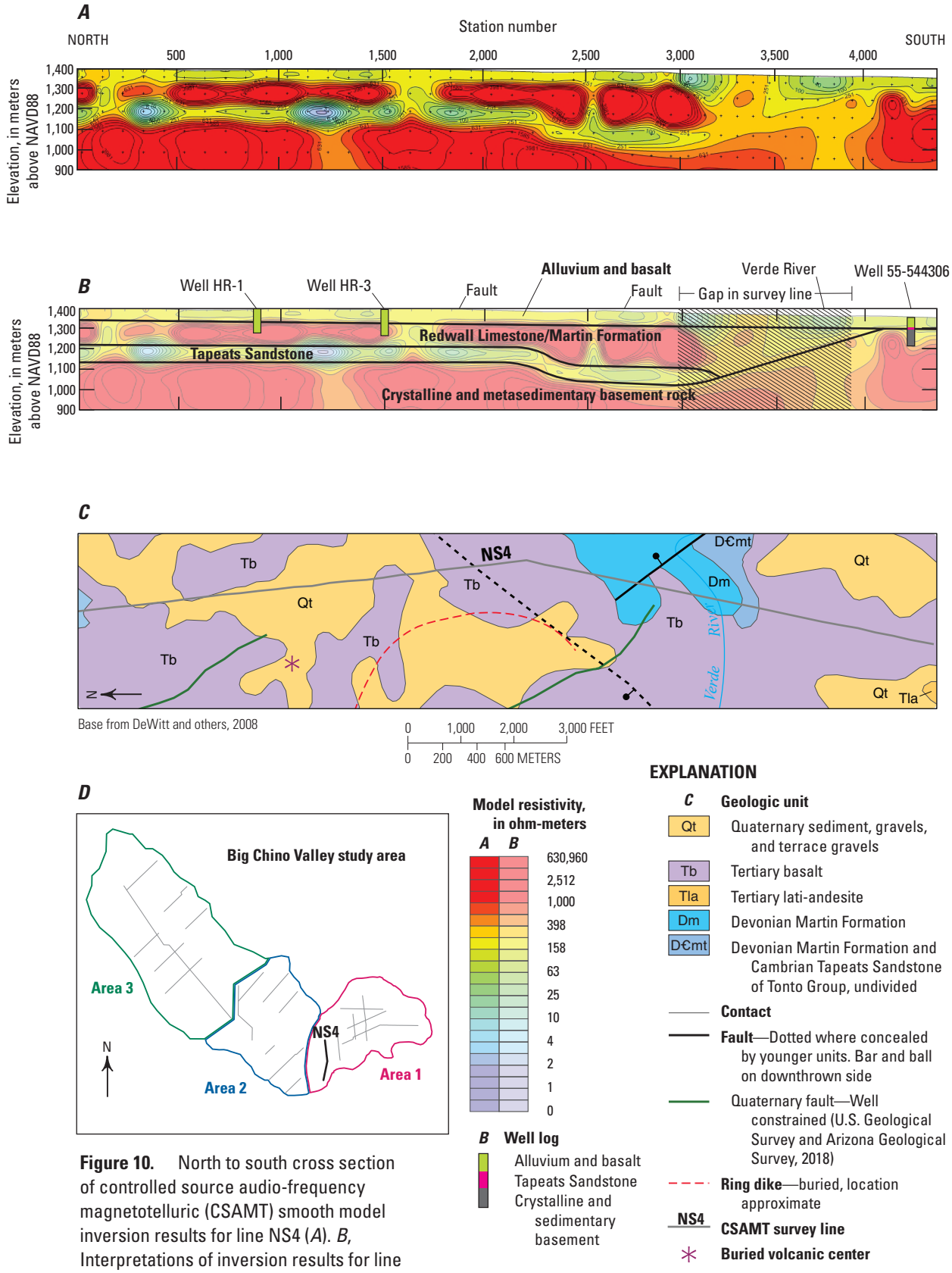

Figure 10. North to south cross section of controlled source audio-frequency magnetotelluric (CSAMT) smooth model inversion results for line NS4 (*A*). *B*, Interpretations of inversion results for line NS4. *C*, Geologic map of area surrounding line NS4 (simplified from DeWitt and others, 2008). *D*, Location map showing survey line NS4 and CSAMT profile, with NS4 in black.

and is interpreted as Paleozoic Redwall Limestone and Martin Formation (figs. 11–13). From 1,220 m to about 1,150 m elevation, there's a more conductive layer, less than 40 ohm-m (purple to green), that is consistent with the Tapeats Sandstone (figs. 11–13). A strong resistor, greater than 250 ohm-m (orange to red), is in the subsurface below an elevation of about 1,150 m which represents granite and schist bedrock (figs. 11, 12 , and 13).

On line EW2 at station 705, the lithologic log of well MW-4b1 maps the subsurface to a depth of 146 m. The log shows that the Supai Formation extends to about 20 m below land surface, and that the Paleozoic Redwall Limestone occurs from about 20 to 70 m below land surface (fig. 12).

Below the Redwall Limestone is the Martin Formation from about 70 m depth to 146 m below land surface. The Supai Formation is represented on line EW2 as less than 100 ohm-m (green to yellow) at the surface to an elevation of 1,320 m (less than 50 m below the surface)(fig. 12). Below this is a layer with greater than 250 ohm-m (yellow to red) below which is consistent with Redwall Limestone and Martin Formation (fig. 12). There is a slightly more conductive unit, less than 40 ohm-m (purple to green), below the Redwall Limestone at an elevation below 1,230 m, which probably represents the Tapeats Sandstone (fig. 12). Resistive material below the conductor, greater than 250 ohm-m, probably represents granite and schist basement rock (fig. 12).

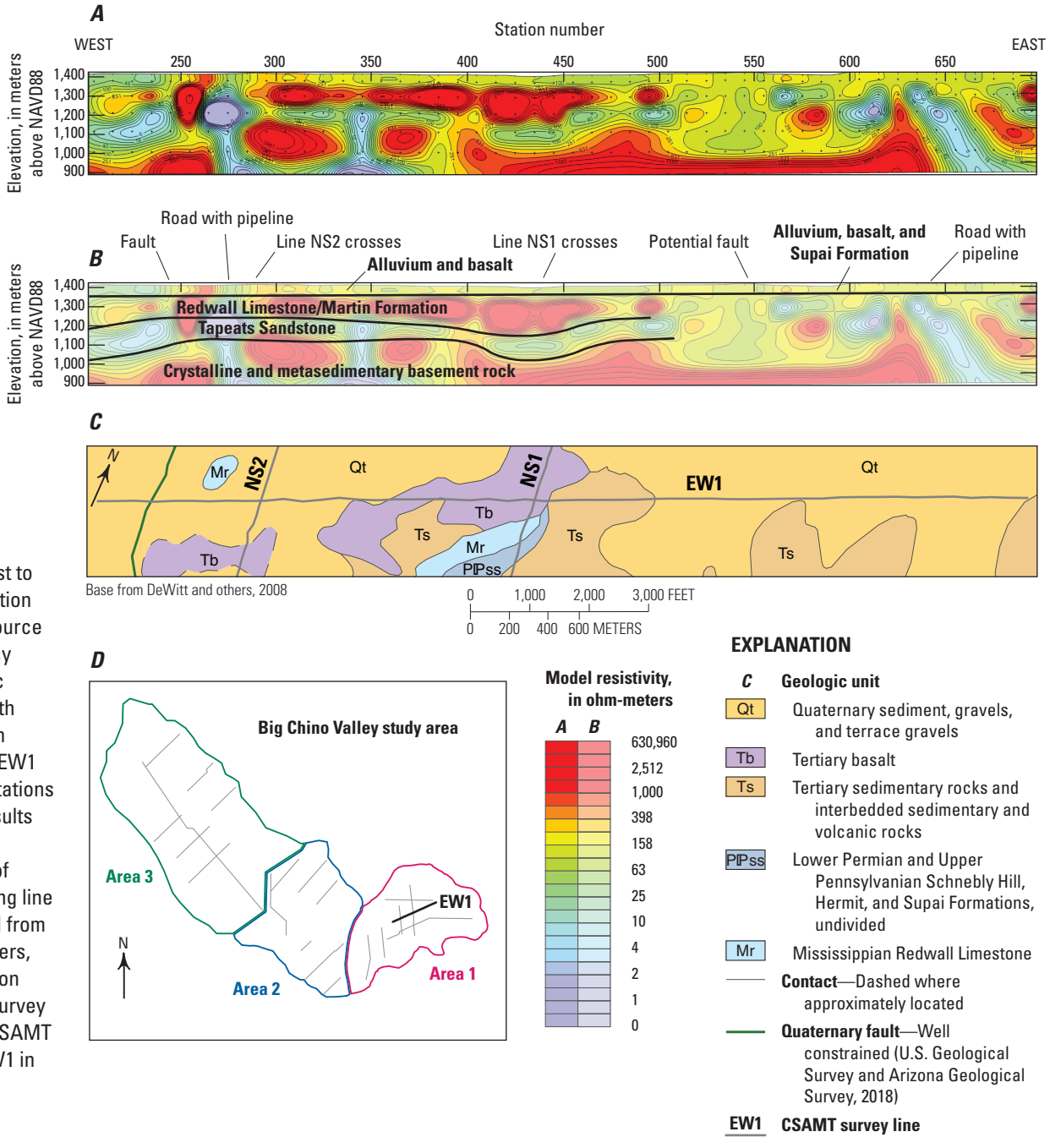

Figure 11. East to west cross section of controlled source audio-frequency magnetotelluric (CSAMT) smooth model inversion results for line EW1 (*A*). *B*, Interpretations of inversion results for line EW1. *C*, Geologic map of area surrounding line EW1 (simplified from DeWitt and others, 2008). *D*, Location map showing survey line EW1 and CSAMT profile, with EW1 in black.

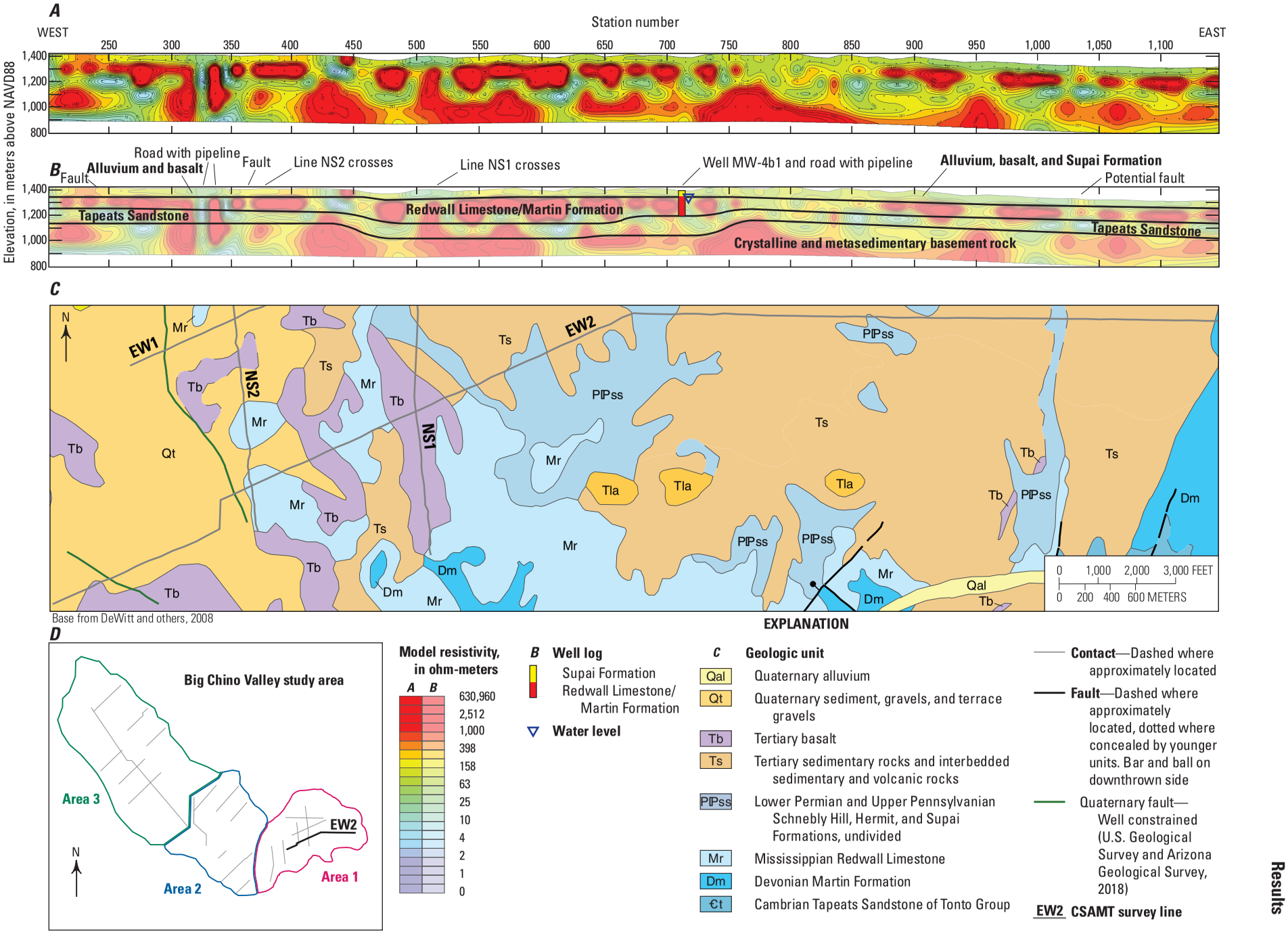

Figure 12. East to west cross section of controlled source audio-frequency magnetotelluric (CSAMT) smooth model inversion results for line EW2 (*A*). *B*, Interpretations of inversion results for line EW2. *C*, Geologic map of area surrounding line EW2 (simplified from DeWitt and others, 2008). *D*, Location map showing survey line EW2 and CSAMT profile, with EW2 in black.

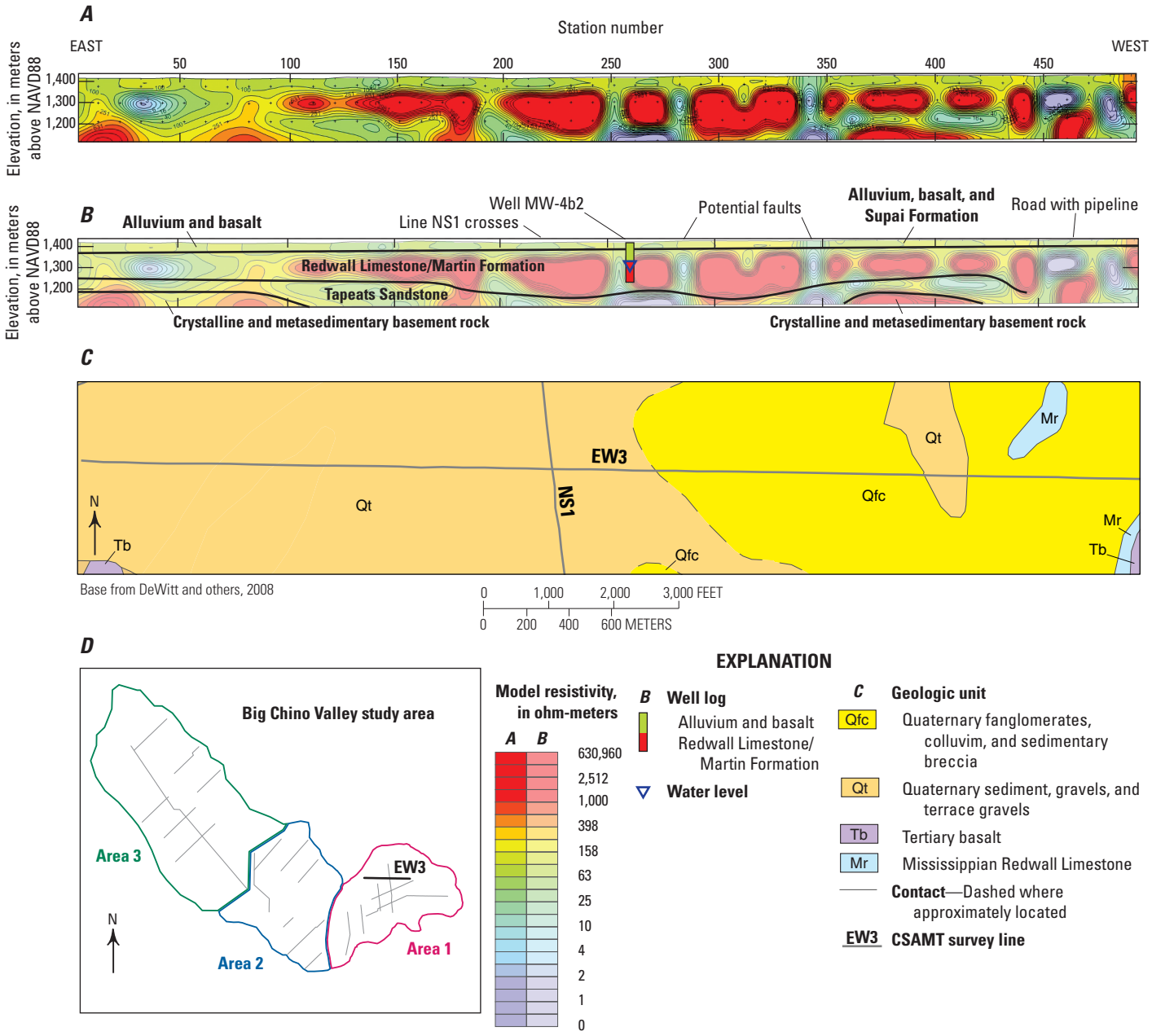

Figure 13. East to west cross section of controlled source audio-frequency magnetotelluric (CSAMT) smooth model inversion results for line EW3 (*A*). *B*, Interpretations of inversion results for line EW3. *C*, Geologic map of area surrounding line EW3 (simplified from DeWitt and others, 2008). *D*, Location map showing survey line EW3 and CSAMT profile, with EW3 in black.

Cultural interference or faulting are evident from anomalies in the EW profiles. Anomalies on line EW1 are found at stations 275, 515 to 615, 635 to 655, and 685. There is a road and a pipeline at station 275 causing some interference and stations 515 to 615 correspond to the area of faults mapped on line NS1 (fig. 11). Stations 635 to 655 are where line EW1 crosses a road, and there appears to also be a pipeline acting as a conductor. Line EW2 also has a number of vertical irregularities, particularly at stations 325, 345, 425, 455, 495, 525, 625, 715, 745, 765 to 865, 945 to 955, and 1025 (fig. 12). Some of these vertical features could be faults, but they could also indicate cultural interference, or they could also be artifacts from the inversion, depending on the horizontal and vertical smoothing coefficients chosen for the inversion. Stations 325 and 345 resemble features that would be produced from buried metal pipes (fig. 12). Station 455 is where line EW2 crosses a power line and there's a road and a buried pipeline near station 525 that could be producing interference (fig. 12). A road crosses line EW2 at station 715 and is most likely the cause of the irregularity at that station (fig. 12). Line EW2 crosses another road at station 1035 (fig. 12). Line EW3 also has areas of potential cultural interference or faulting, at stations 195, 255, 285, 345, and 455 to 485 (fig. 13).

Area 2

Area 2 encompasses CSAMT lines GS6, GS8, GS16, FM, FME, FMW, and NS5. Area 2 is a transition between area 1, where alluvium is thin to nonexistent, and area 3, where alluvium is so deep that it exceeds the depth of our profiles. Lines in area 2 are generally more conductive than in area 1 and have some highly resistive units toward the bottom of the profiles that indicate presence of Paleozoic sedimentary rocks. Depths of investigation in area 2 are generally a few hundred meters. The average alluvium thickness in area 2 is about 100 to 200 m. Some of the lines in area 2 are near the basin margin where the alluvium is thinnest.

Survey lines GS6, GS8, and GS16 are on land adjacent to or lands leased by the Gunsite Academy near Paulden. Inverted resistivity modeling of these three lines indicates that the subsurface here has two main layers: an upper layer of material, 1,000 ohm-m or less (green and purple in fig. 14–16) at an elevation above 1,250 m, and a lower layer below 1,250 m elevation of resistive material, greater than 100 ohm-m (yellow-red in figs. 14–16). The two layers are interpreted to be alluvium and basalt in the upper layer and Redwall Limestone and Martin Formation in the lower layer. The southwest end of line GS8, starting at station 4450, does not appear to show two layers, but instead is a single layer of 40 to 60 ohm-m material (fig. 15). There are two mapped faults to the northwest and

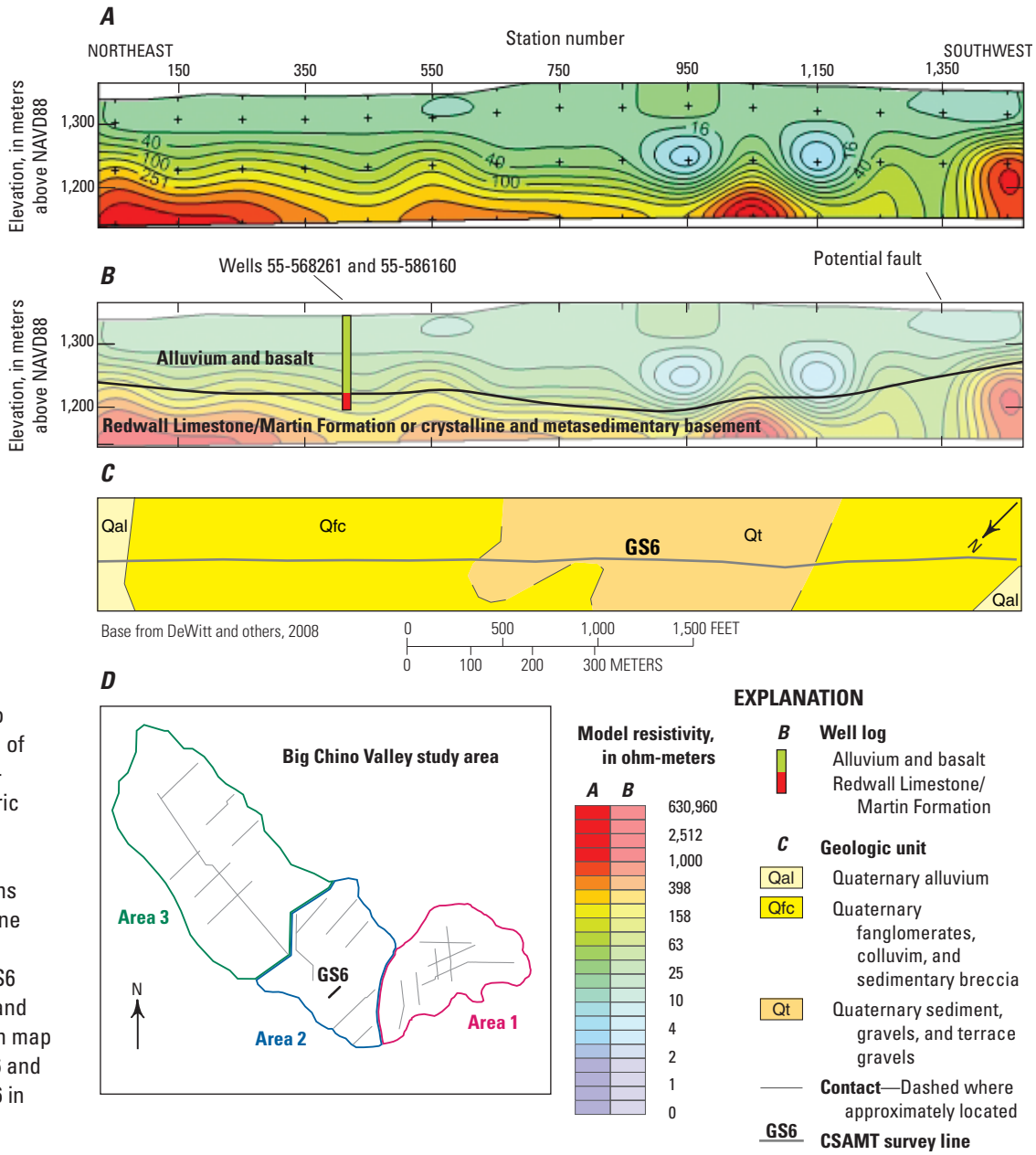

Figure 14. Northeast to southwest cross section of controlled source audio-frequency magnetotelluric (CSAMT) smooth model inversion results for line GS6 (*A*). *B*, Interpretations of inversion results for line GS6. *C*, Geologic map of area surrounding line GS6 (simplified from DeWitt and others, 2008). *D*, Location map showing survey line GS6 and CSAMT profile, with GS6 in black.

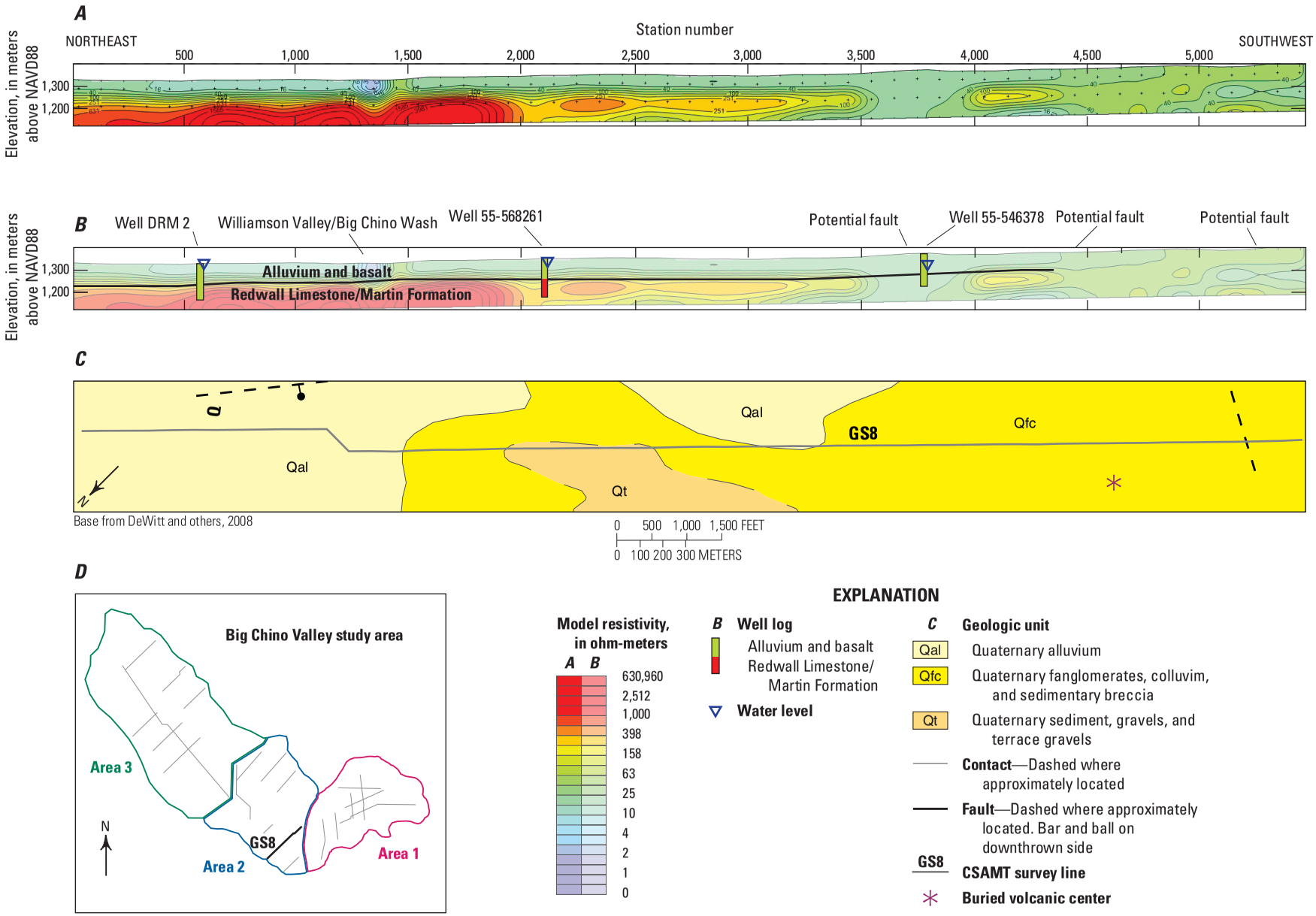

Figure 15. Northeast to southwest cross section of controlled source audio-frequency magnetotelluric (CSAMT) smooth model inversion results for line GS8 (*A*). *B*, Interpretations of inversion results for line GS8. *C*, Geologic map of area surrounding line GS8 (simplified from DeWitt and others, 2008). *D*, Location map showing survey line GS8 and CSAMT profile, with GS8 in black.

southeast of line GS8 that project into station 4450 (fig. 15), as well as a previously mapped fault between stations 3650 and 3750 (fig. 15) (DeWitt and others, 2008). Mapped faults are present on line GS16 at station 950, and the resistivity plot shows a distinct anomaly at station 950 (fig. 16). There also appears to be an unmapped fault near stations 2150 and 2250 on GS16 (fig. 16).

Lines FM, FME, and FMW are in the area of "Feather Mountain," a locally named hill at the southeast end of Big Black Mesa, and are primarily comprised of conductive material, less than 20 ohm-m (purple to green), with some resistive material, greater than 200 ohm-m, at the bottom of the northeast side of lines FM and FME (figs. 17, 18, and 19). The upper conductive layer is consistent with alluvial basin fill and the lower unit consistent with Paleozoic Martin and Redwall Limestones. Lines FM and FME intersect the Big Chino Fault and other faults associated with it. The resistive material seen in the inversion model is consistent with Paleozoic

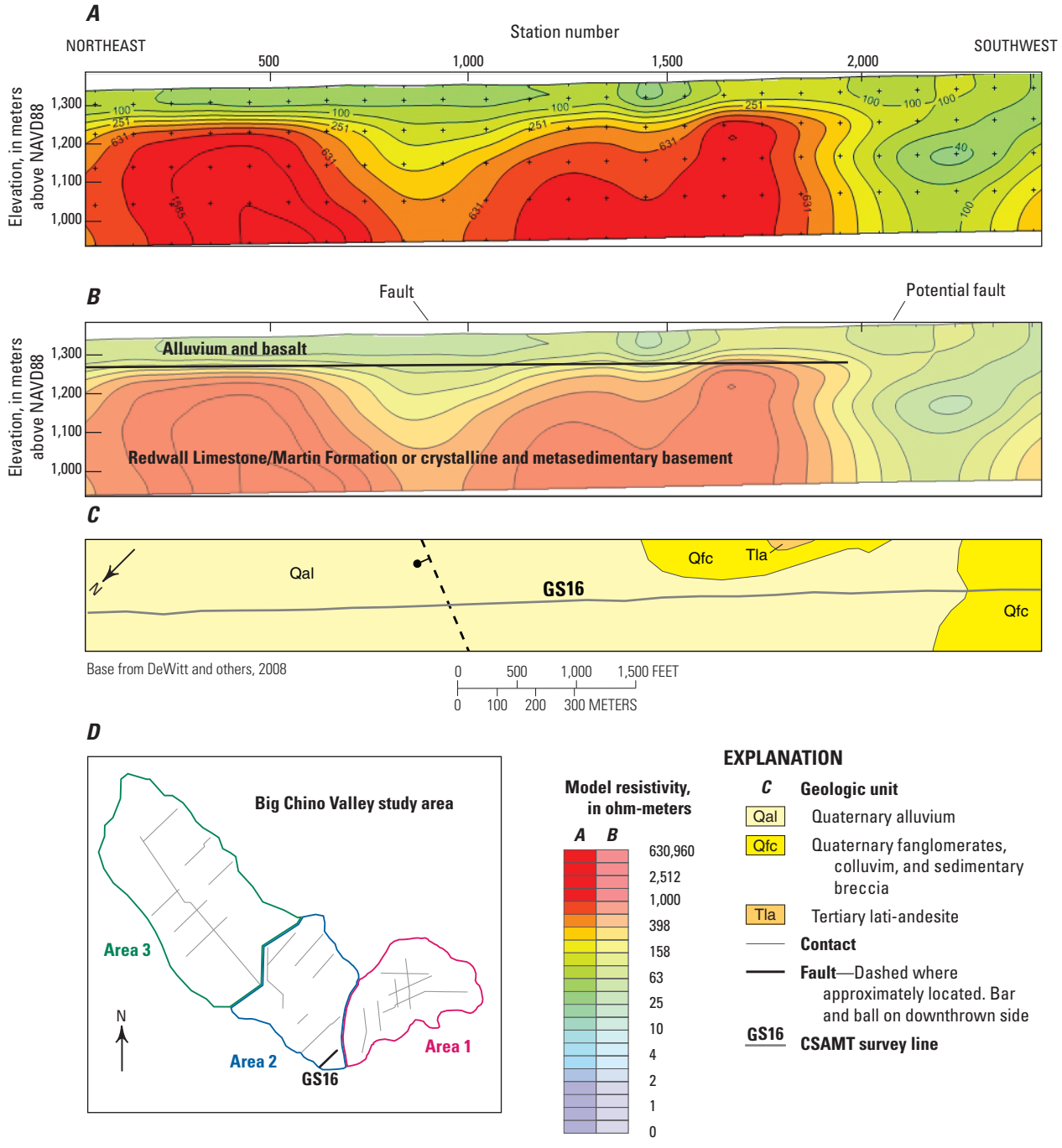

Figure 16. Northeast to southwest cross section of controlled source audio-frequency magnetotelluric (CSAMT) smooth model inversion results for line GS16 (*A*). *B*, Interpretations of inversion results for line GS16. *C*, Geologic map of area surrounding line GS16 (simplified from DeWitt and others, 2008). *D*, Location map showing survey line GS16 and CSAMT profile, with GS16 in black.

limestones juxtaposed against alluvial basin fill. On line FM, the Big Chino Fault is mapped at about station 950 (fig. 17). This normal fault is observed in the subsurface on line FM from about station 650 to 2150 where conductive (purple to green) material overlies resistive (yellow to red) material (fig. 17). On line FME, there are two areas where mapped faults cross the profile, at station 150 and station 1450, and one area where a mapped fault projects into the profile, at station 2450 (fig. 18). The resistivity profile from line FME shows an irregularity closer to station 1750 than 1450, but based on the inversion results there is a potential fault at station 2450 (fig. 18). The subsurface profile beneath line FMW is relatively homogenous with a conductive layer at the surface, less than 20 ohm-m (purple to green), that extends down to about 1,300 m elevation (fig. 19). A second, more conductive, layer can be found below 1,300 m with resistivity values less than 10

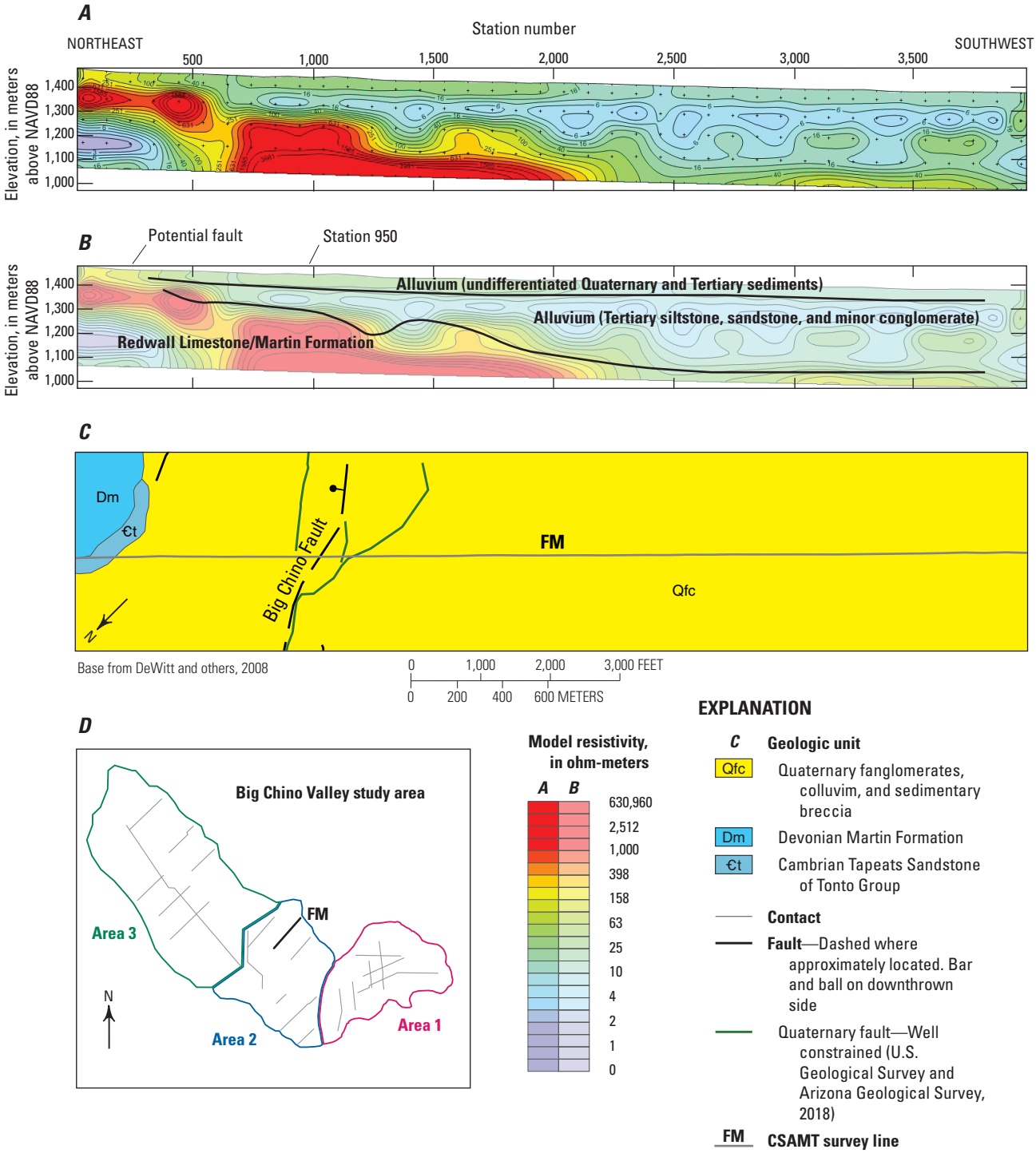

Figure 17. Northeast to southwest cross section of controlled source audio-frequency magnetotelluric (CSAMT) smooth model inversion results for line FM (*A*). *B*, Interpretations of inversion results for line FM. *C*, Geologic map of area surrounding line FM (simplified from DeWitt and others, 2008). *D*, Location map showing survey line FM and CSAMT profile, with FM in black.

ohm-m (purple) (fig. 19). This lower layer, with very conductive properties, shows the extent and thickness of the silt and clay in the area.

Line NS5 is south of the Feather Mountain lines (FM, FME, and FMW) and intersects line FMW at NS5 station 1850 and FMW station 4450 (figs. 19 and 20). Line NS5 is two line segments that are offset, but combined into a single line for inversion. Line NS5 is similar to line FMW in resistivity structure, being relatively homogenous with a conductive layer at the surface, less than 20 ohm-m (purple to green), that extends down to about 1,300 m elevation (fig. 20). A second, more conductive, layer below 1,300 m has resistivity values less than 10 ohm-m (purple, fig. 20). These two layers are consistent with alluvial basin fill, where the more conductive layer is basin fill with higher clay or silt content. An anomaly near stations 1850 and 1950 indicates that some resistive material (yellow) is adjacent to conductive material (purple to blue), which could be a buried fault (fig. 20). That same resistive material (yellow) in line NS5 can be seen in line FMW at station 4450 (figs. 19 and 20). In the southern part of line NS5, between station 5050 and 6450, there is resistive material, greater than 20 ohm-m (green to yellow), at the bottom of the plot below 1,200 m elevation, which is interpreted as Redwall Limestone/Martin Formation (fig. 20).

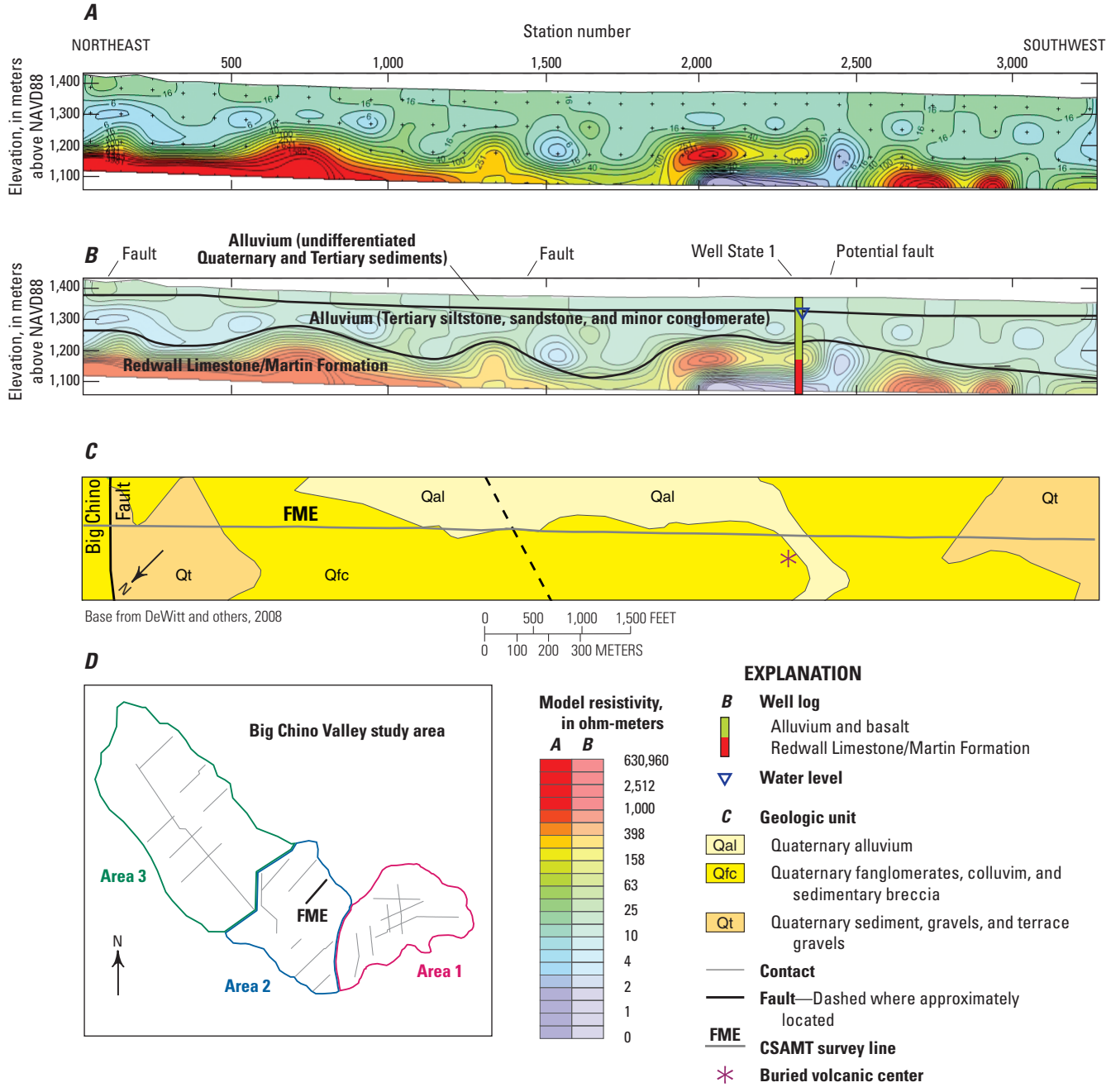

Figure 18. Northeast to southwest cross section of controlled source audio-frequency magnetotelluric (CSAMT) smooth model inversion results for line FME (*A*). *B*, Interpretations of inversion results for line FME. *C*, Geologic map of area surrounding line FME (simplified from DeWitt and others, 2008). D, Location map showing survey line FME and CSAMT profile, with FME in black.

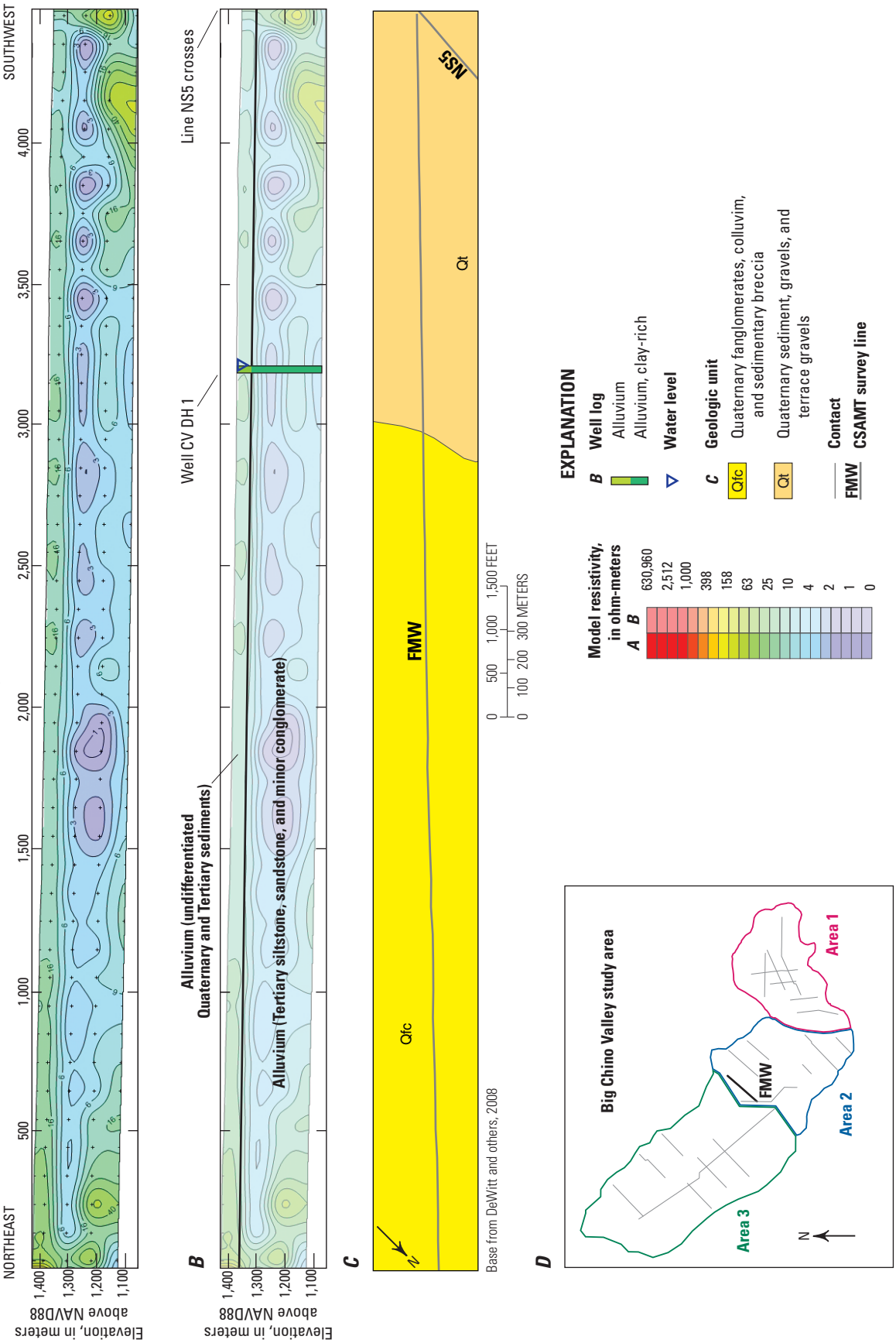

Figure 19. Northeast to southwest cross section of controlled source audio-frequency magnetotelluric (CSAMT) smooth model inversion results for line FMW (*A*). *B*, Interpretations of inversion results for line FMW. *C*, Geologic map of area surrounding line FMW (simplified from DeWitt and others, 2008). *D*, Location map showing survey line FMW and CSAMT profile, with FMW in black.

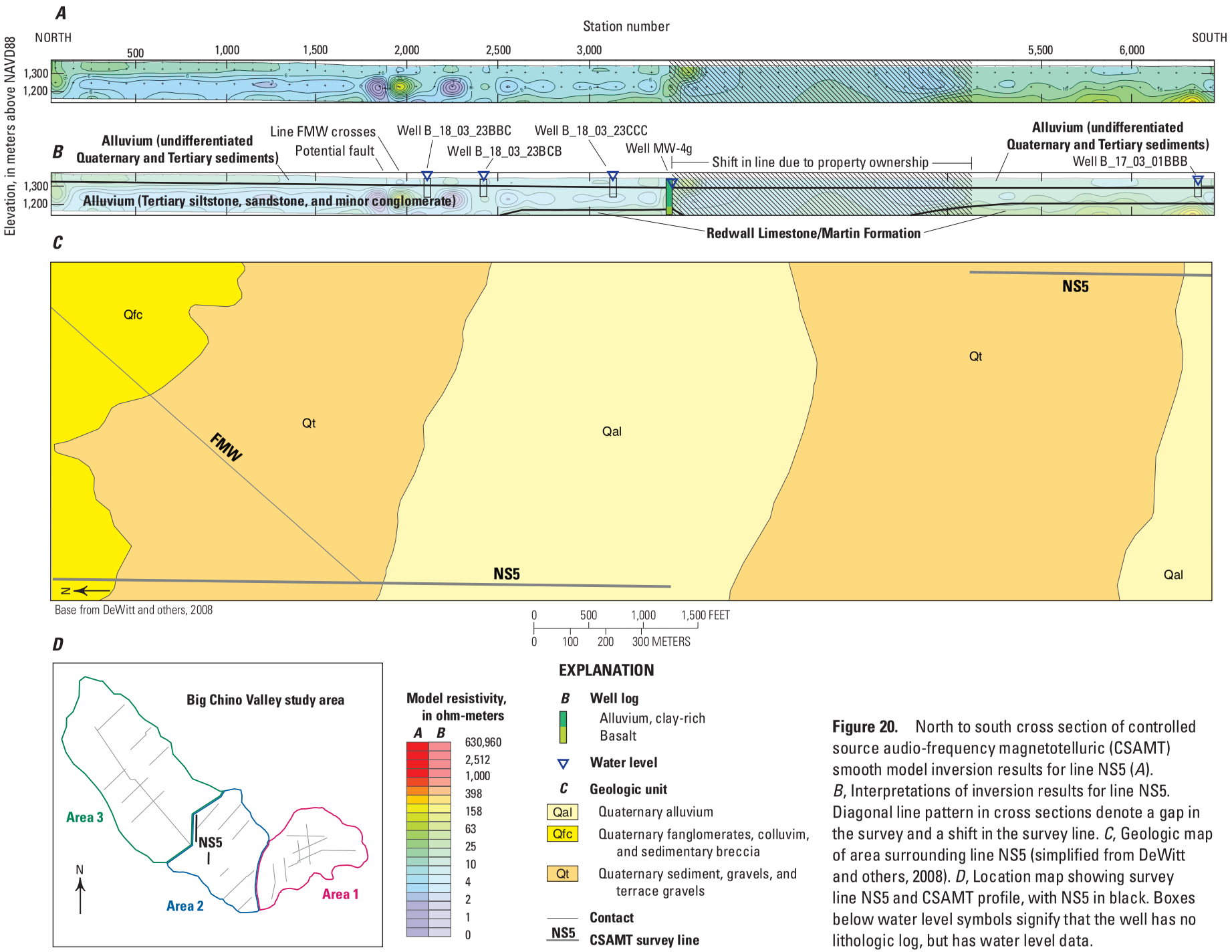

Figure 20. North to south cross section of controlled source audio-frequency magnetotelluric (CSAMT) smooth model inversion results for line NS5 (*A*). *B*, Interpretations of inversion results for line NS5. Diagonal line pattern in cross sections denote a gap in the survey and a shift in the survey line. *C*, Geologic map of area surrounding line NS5 (simplified from DeWitt and others, 2008). *D*, Location map showing survey line NS5 and CSAMT profile, with NS5 in black. Boxes below water level symbols signify that the well has no lithologic log, but has water level data.

Area 3

Area 3 encompasses CSAMT lines AX, K1, WC, WCN, CG, CH, and WR. The geology of area 3 is primarily alluvial basin fill, specifically Tertiary to Quaternary sedimentary rocks, and Tertiary basalt. The rocks in area 3 are generally more conductive than in areas 1 and 2, and have few highly resistive units that indicate the presence of Paleozoic sedimentary rocks. Because of this more conductive material, depths of investigation are generally shallower than areas 1 and 2, to only about 300 m below land surface.

Line AX follows the axis of the Big Chino subbasin and is 20 km long, the longest of any of the CSAMT profiles (fig. 21). Inversion results from line AX show conductive material across the entire profile and that most of the material is less than 20 ohm-m (purple to blue-green in fig. 21). There's a strong conductor, less than 5 ohm-m, in the center of the profile from about station 550 to 8950, at an elevation between 1,150 and 1,250 m (fig. 21). The strong conductor appears to dip to the northwest, and so northwest of station 8950 it is below the bottom of the profile at 1,100 m elevation.

Lines K1, WC, and WCN are located on the southwest side of the Big Chino subbasin and are mainly underlain by conductive material, less than 20 ohm-m (purple to blue-green in figs. 22, 23, and 24). Lines K1 and WC are very similar, having primarily material less than 20 ohm-m throughout the profile (figs. 22 and 23). Both lines show a resistor in the southwest portion of the plot at an elevation of about 1,250 m (figs. 22 and 23). On line K1 the resistor (yellow to red, fig. 22) is between stations 50 and 1750, and on line WC the resistor (yellow) is between stations 50 and 450 (fig. 23). Line WCN is unique among these three lines, having layers of resistive material, 600 to 4,000 ohm-m (yellow to red in fig. 24), interbedded within the conductive, 20 ohm-m material (blue-green to purple, fig. 24). The Paleozoic Martin Formation outcrops just north and west of line WCN and may be contributing to some of the resistive signal. Line WCN has about 100 to 150 m of conductive material, less than 20 ohm-m (purple to green, fig. 24), at the surface. Below the conductor is a strong resistor, in some areas greater than 1,000 ohm-m (yellow to red, fig. 24), ranging in thickness from 100 to 300 m at an elevation of about 1,200 m (fig. 24). A moderate conductor, below an elevation of 1,100 m, has resistivity values less than 40 ohm-m (fig. 24). The deepest part of the profile along line WCN consists of a strong resistor at an elevation below 800 m (fig. 24). There are also a number of features within line WCN that resemble faults. Between stations 650 and 850, at station 1550, and at station 3550 there are significant breaks in the resistive layer that could be faults (fig. 24).

Lines CG, CH and WR are similar to one another and mainly comprised of conductive material less than 20 ohm-m (purple to blue-green, figs. 25, 26, and 27). These three CSAMT lines are located on the northeast side of the Big Chino subbasin. The inverted section profiles suggest that there are four distinct subsurface layers in this area, except around line WR, which only shows three layers. The first layer is at the surface, 16 ohm-m or less (blue-green in figs. 25–27), and is 50 m thick. The second layer is a more conductive, 6 ohm-m or less (purple, figs. 25–27), and is also about 50 m thick. The third layer is the most resistive of these lines, about 40 ohm-m (yellow-green, figs. 25–27), and is about 50 m thick. The bottom layer is a strong conductor, 6 ohm-m or less (purple, figs. 25 and 26). The lithologic log from well CVM_1 indicates that basalt is present at depth, and so the third layer, of 40 ohm-m material, could represent the basalt in the basin.

Line WR is distinct from lines CG and CH because there is a resistor at depth, about 1,250 m elevation, that occurs between stations 3000 and 3500 (fig. 27). Line WR also crosses the Big Chino Fault at station 4750, and in the inversion profile the fault is evident where conductive and resistive material is juxtaposed (fig. 27).

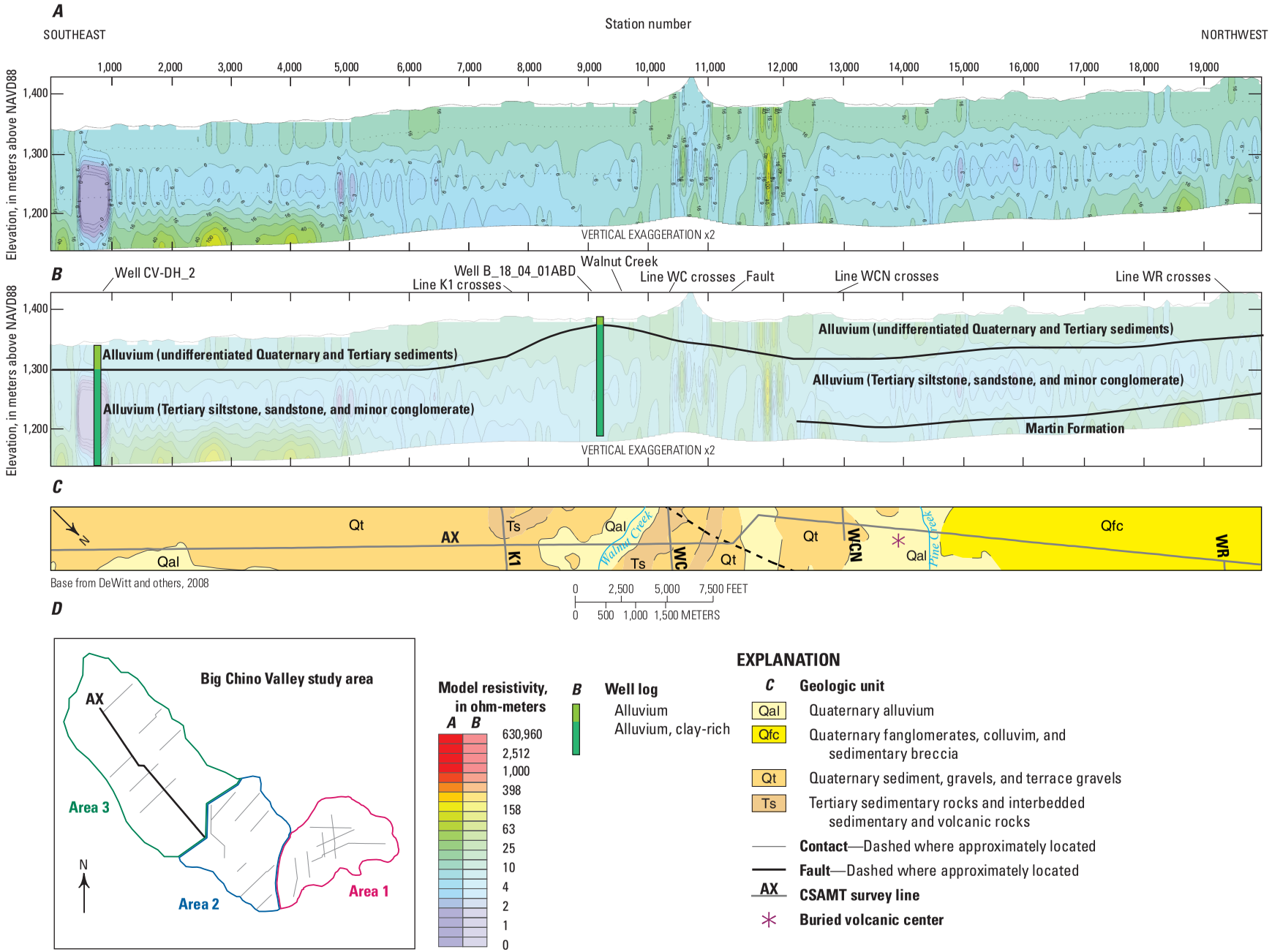

Figure 21. Southeast to northwest cross section of controlled source audio-frequency magnetotelluric (CSAMT) smooth model inversion results for line AX (*A*). *B*, Interpretations of inversion results for line AX. *C*, Geologic map of area surrounding line AX (simplified from DeWitt and others, 2008). D, Location map showing survey line AX and CSAMT profile, with AX in black.

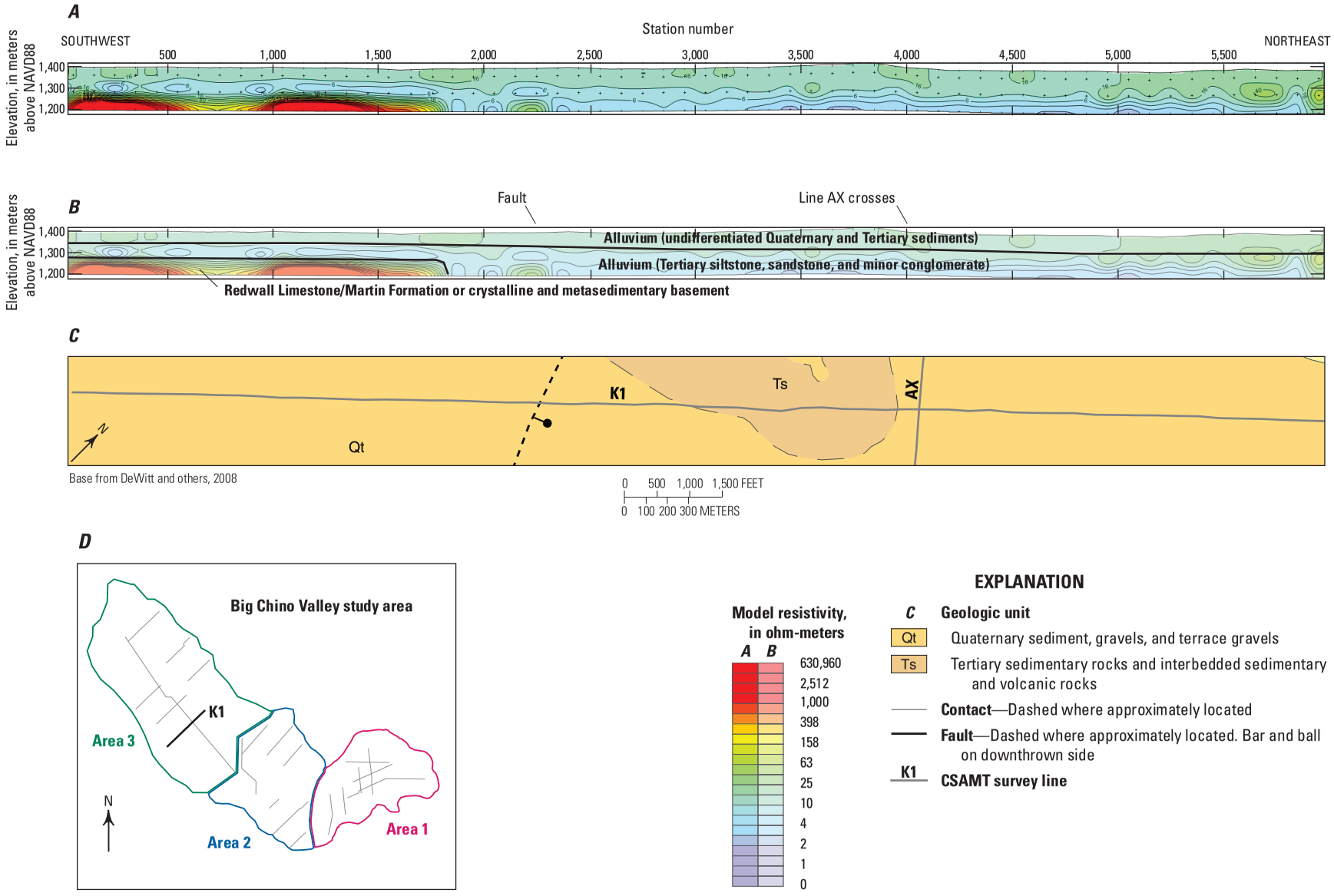

Figure 22. Southwest to northeast cross section of controlled source audio-frequency magnetotelluric (CSAMT) smooth model inversion results for line K1 (*A*). *B*, Interpretations of inversion results for line GS6. *C*, Geologic map of area surrounding line K1 (simplified from DeWitt and others, 2008). *D*, Location map showing survey line K1 and CSAMT profile, with K1 in black.

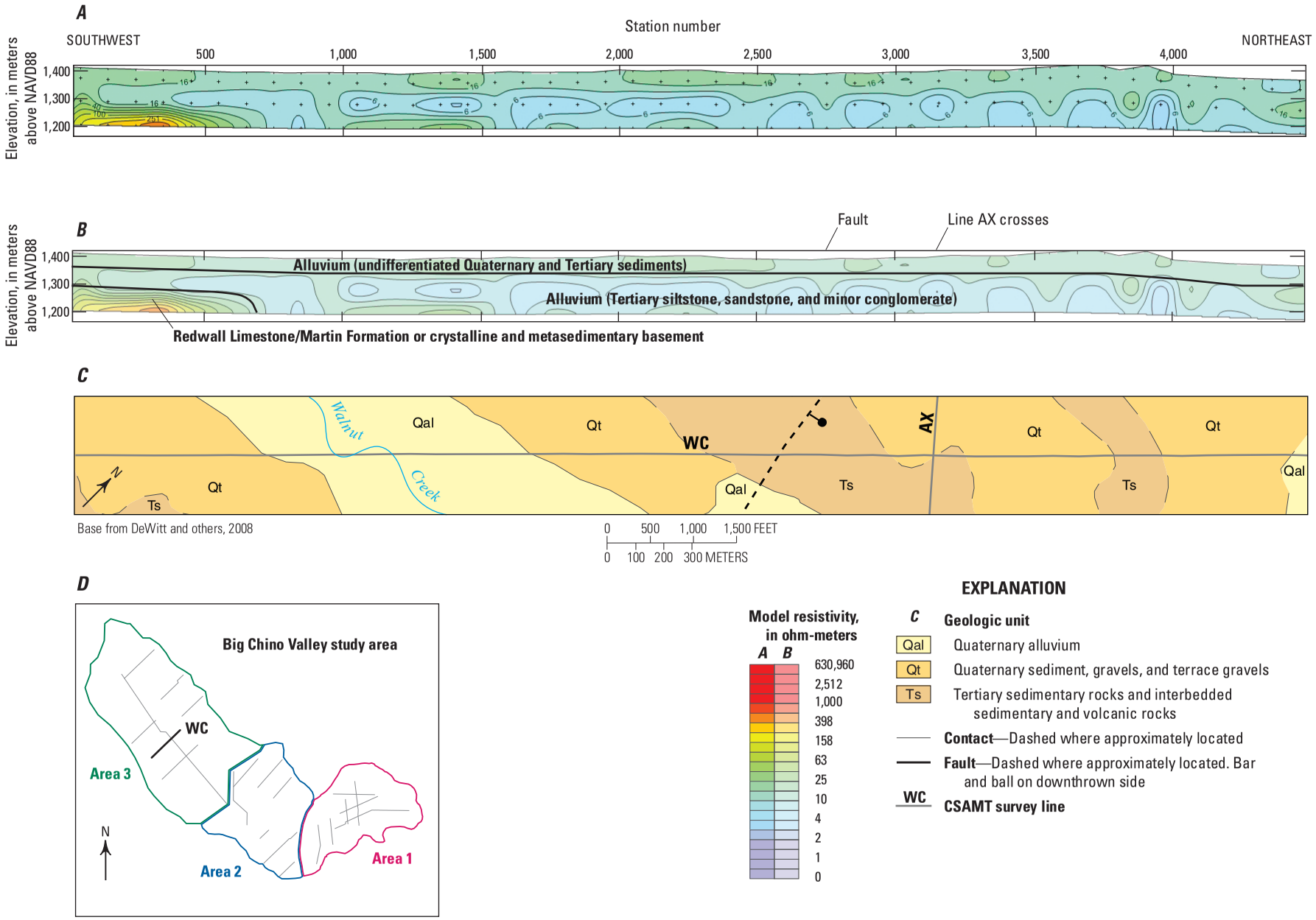

Figure 23. Southwest to northeast cross section of controlled source audio-frequency magnetotelluric (CSAMT) smooth model inversion results for line WC (*A*). *B*, Interpretations of inversion results for line WC. *C*, Geologic map of area surrounding line WC (simplified from DeWitt and others, 2008). *D*, Location map showing survey line WC and CSAMT profile, with WC in black.

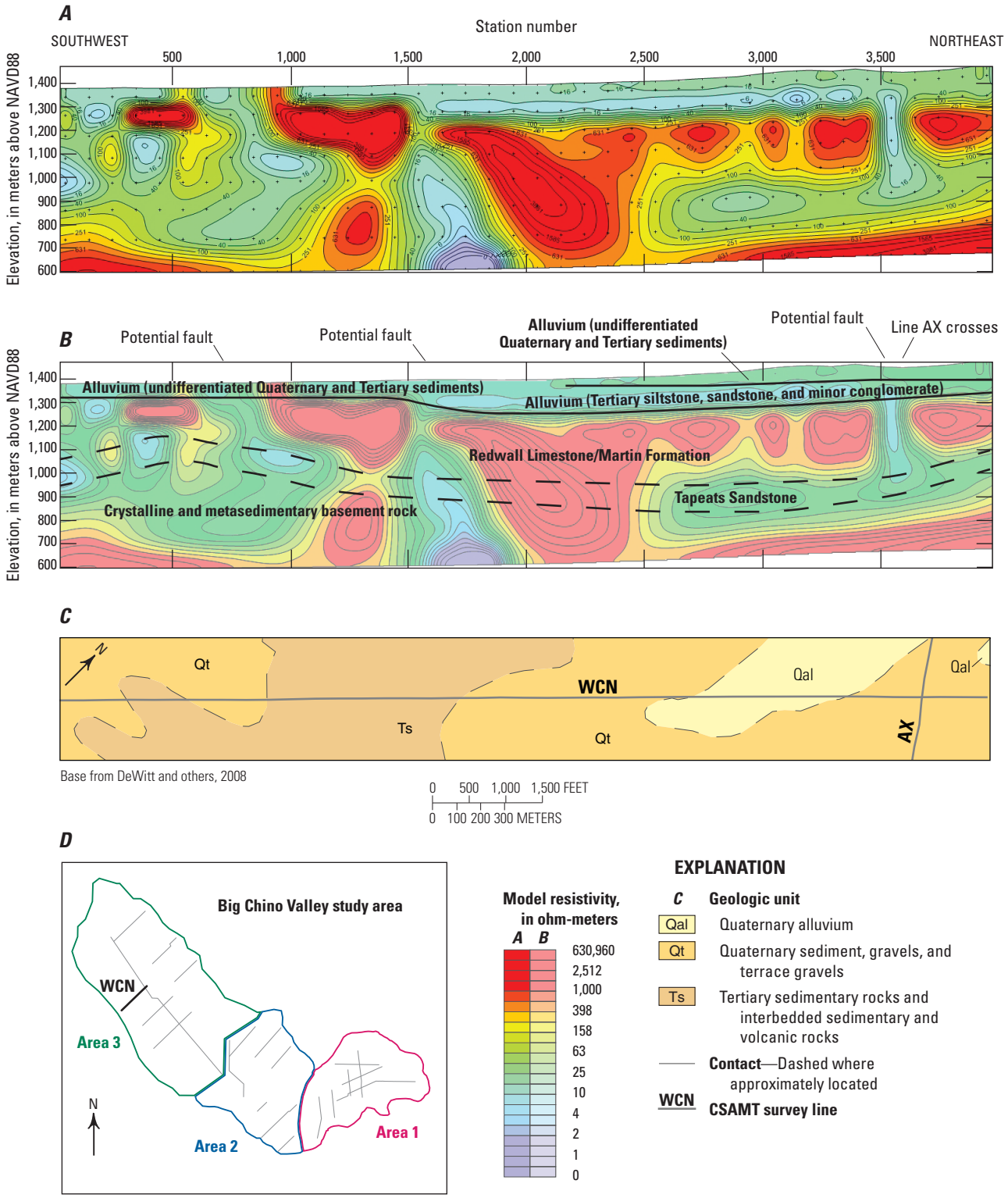

Figure 24. Southwest to northeast cross section of controlled source audio-frequency magnetotelluric (CSAMT) smooth model inversion results for line WCN (*A*). *B*, Interpretations of inversion results for line WCN. *C*, Geologic map of area surrounding line WCN (simplified from DeWitt and others, 2008). *D*, Location map showing survey line WCN and CSAMT profile, with WCN in black.

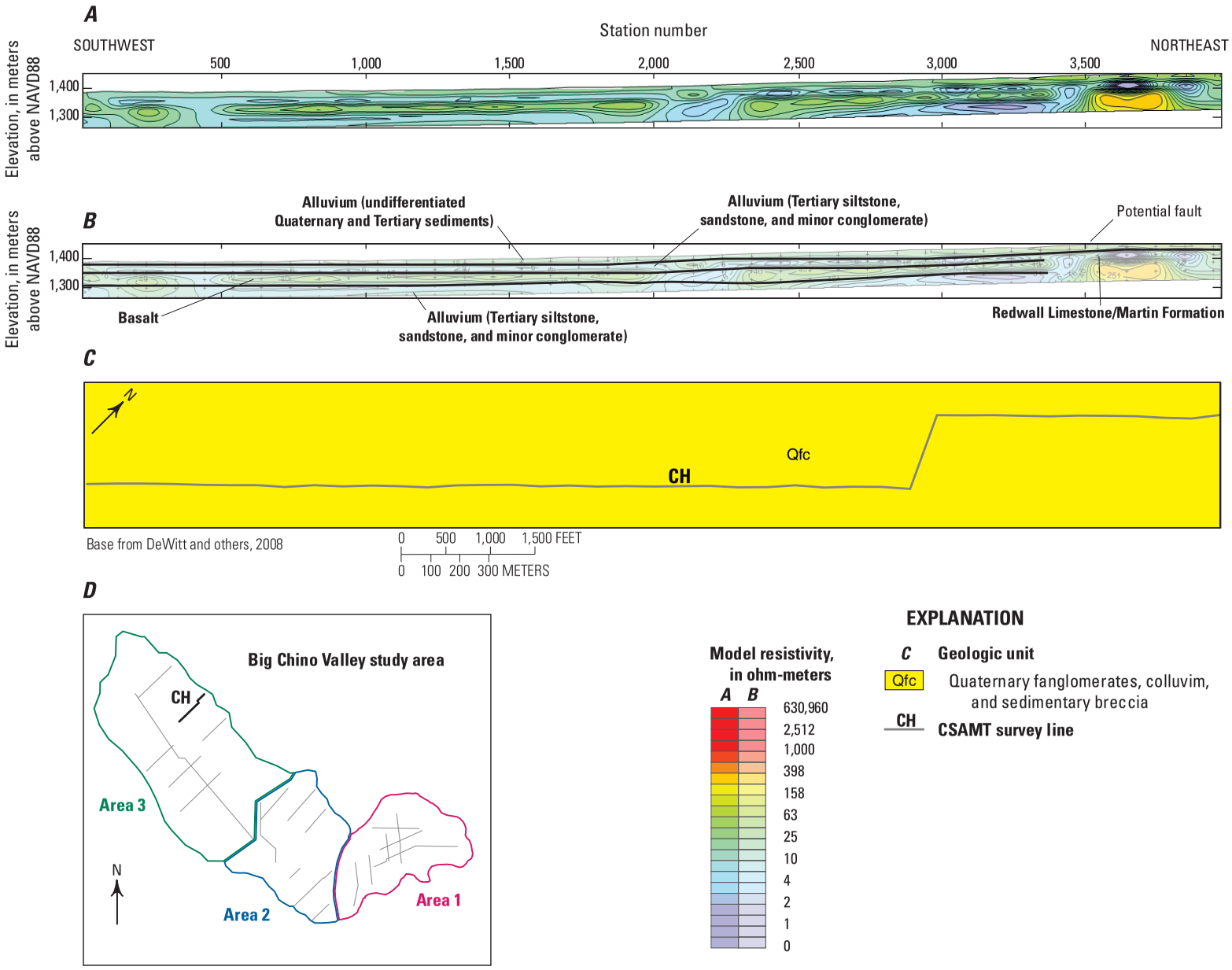

Figure 25. Southwest to northeast cross section of controlled source audio-frequency magnetotelluric (CSAMT) smooth model inversion results for line CG (*A*). *B*, Interpretations of inversion results for line CG. *C*, Geologic map of area surrounding line CG (simplified from DeWitt and others, 2008). *D*, Location map showing survey line CG and CSAMT profile, with CG in black.

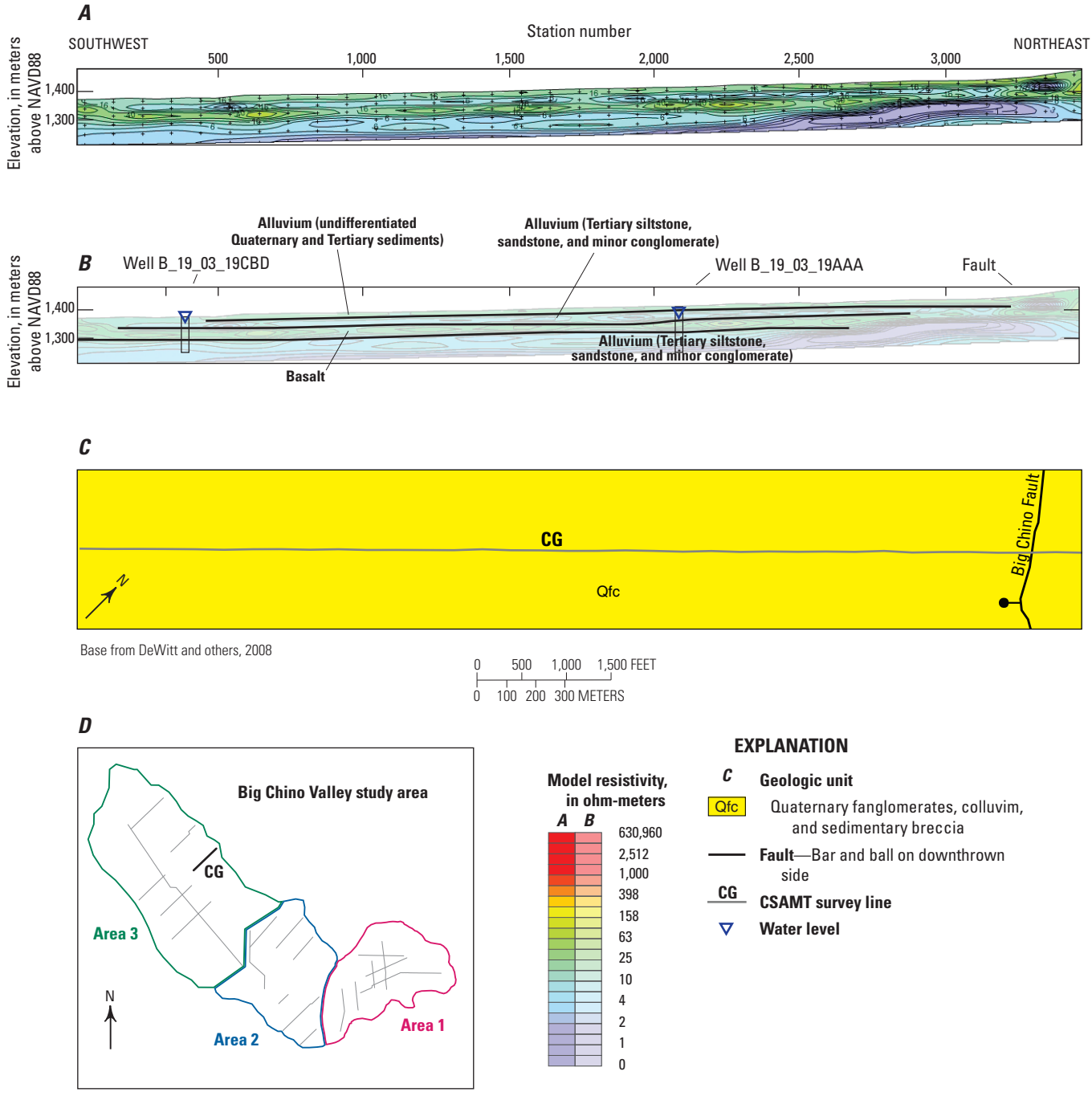

Figure 26. Southwest to northeast cross section of controlled source audio-frequency magnetotelluric (CSAMT) smooth model inversion results for line CH (*A*). *B*, Interpretations of inversion results for line CH. Water-level data are from lithologic logs of wells B_19_03_19CBD and B_19_03_19AAA. *C*, Geologic map of area surrounding line CH (simplified from DeWitt and others, 2008). *D*, Location map showing survey line CH and CSAMT profile, with CH in black. Boxes below water level symbols signify that the well has no lithologic log, but has water level data.

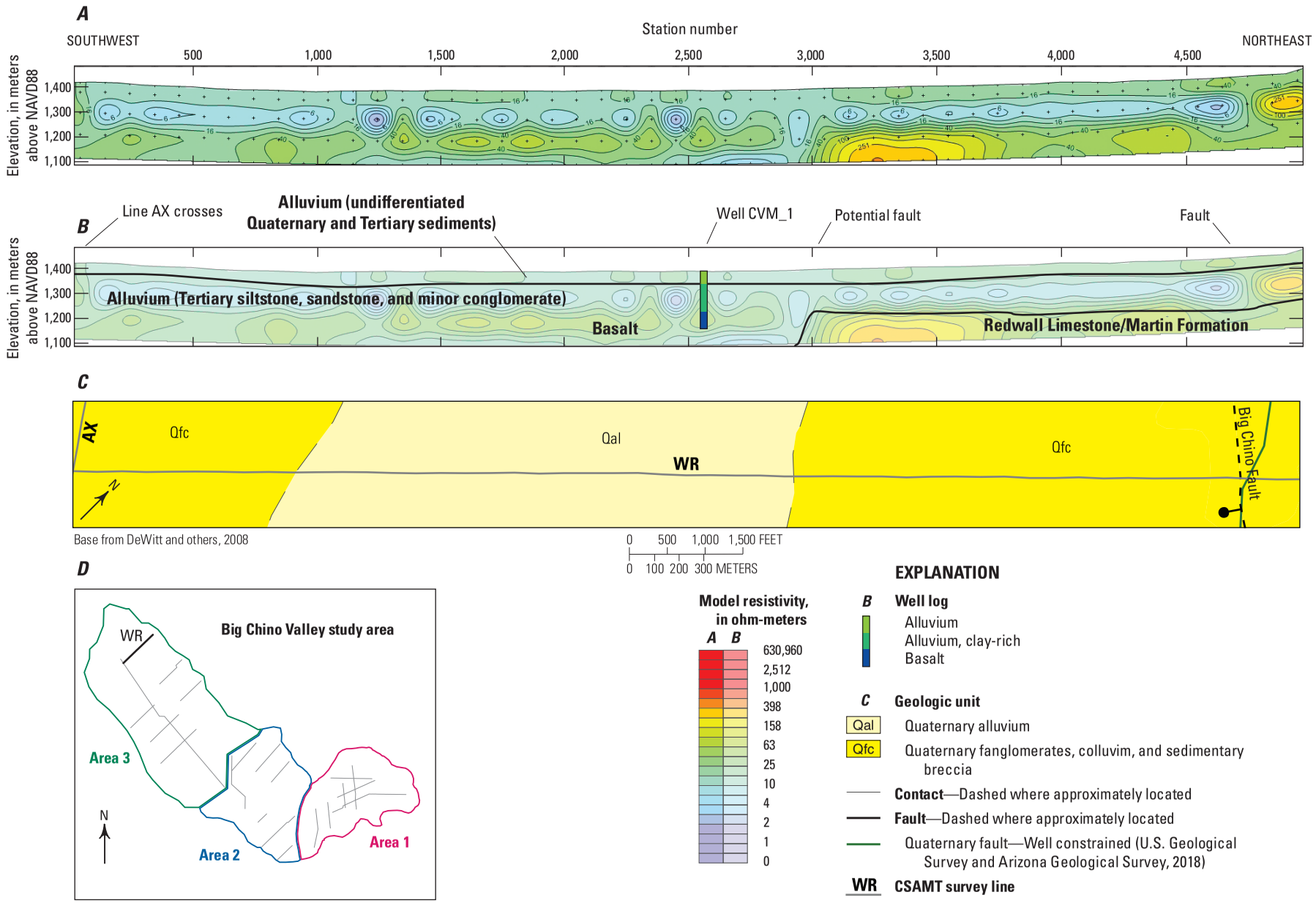

Figure 27. Southwest to northeast cross section of controlled source audio-frequency magnetotelluric (CSAMT) smooth model inversion results for line WR (*A*). *B*, Interpretations of inversion results for line WR. *C*, Geologic map of area surrounding line WR (simplified from DeWitt and others, 2008). *D*, Location map showing survey line WR and CSAMT profile, with WR in black.

Summary

The main water-bearing stratigraphic unit in the Big Chino subbasin near Paulden is Tertiary alluvial-fill sediments. The Devonian Martin Formation (dolomite, limestone, sandy siltstone) also yields some water to wells near Drake, a little northeast of Big Chino subbasin. The Mississippian Redwall Limestone, considered highly permeable, provides water to wells in the Paulden area, and to wells east of the Big Chino subbasin.

We used CSAMT, a low-impact, non-intrusive, electrical-resistance geophysical technique, to evaluate the subsurface stratigraphy of the Big Chino subbasin near Paulden. Specifically, the purpose of the CSAMT surveys was to improve the conceptual model of the aquifer by constraining the basin geometry and identifying stratigraphic units. Twenty-one electromagnetic surveys were conducted in three designated geographic areas of the basin for a total of 100 km (62.1 mi) of CSAMT survey lines. Fourteen survey lines were west of the town of Paulden and the other seven were east of Paulden. Data were inverted to provide a two-dimensional resistivity profile for each survey line and final inversion models represent the best fit to measured data.

CSAMT lines west of Paulden are consistent with the presence of thicker alluvial basin deposits that range from 100 m thick to a few hundred meters thick. CSAMT lines east of Paulden are consistent with thinner alluvial and basalt deposits overlying Paleozoic Martin Formation and Redwall Limestone, Tapeats Sandstone, and Precambrian granite and schist.

Electromagnetic surveys were conducted in three areas in the Big Chino Subbasin near Paulden, Arizona: area 1 east of Paulden, area 2 west of but near the housing development in Paulden, and area 3 west and northwest of Paulden (fig. 2). The results of the CSAMT surveys indicate that area 1 has complex geology that includes layers of Quaternary and Tertiary alluvium and basalt near the surface, overlying Paleozoic Supai Formation, Redwall Limestone, Martin Formation, Tapeats Sandstone, and Precambrian crystalline basement rocks (DeWitt and others, 2005; Blasch and others, 2006). The electrical properties of basalt and Paleozoic limestone can be difficult to differentiate because they are both electrically resistive, especially when the limestone occurs as a thin layer at the surface. Area 2 is a transition between area 1, where alluvium is thin to nonexistent, and area 3, where alluvium is so deep that it exceeds the depth of our profiles. The subsurface rocks in area 2 are generally more conductive than in area 1, and there are some highly-resistive units towards the bottom of the profiles that indicate the presence of Paleozoic sedimentary rocks. Depths of investigation in area 2 are generally a few hundred meters. The average alluvium thickness in area 2 is about 100 to 200 m. Some of the lines in area 2 are near the basin margin where the alluvium is thinnest. The subsurface rocks in area 3 are generally more conductive than in areas 2 and 3, and there are few highly resistive units that indicate the presence of Paleozoic sedimentary rocks. Because of this more conductive material, depths of investigation are generally more shallow, to about 300 m below land surface.

References Cited

Arizona Department of Water Resources, 2000, Verde River watershed study: Arizona Department of Water Resources, 483 p., accessed March 15, 2018, at http://www.verderiverinstitute.org/200004%20DWR%20Verde%20River%20Watershed%20Report.pdf.

Arizona Department of Water Resources, 2014a, Verde River Basin: Arizona Department of Water Resources, Arizona Water Atlas, section 5.5, p. 240–329, accessed on March 15, 2018, at http://www.azwater.gov/AzDWR/StatewidePlanning/WaterAtlas/CentralHighlands/documents/volume_5_VRB_final.pdf.

Arizona Department of Water Resources, 2014b, Central Highlands planning area water supply—groundwater: Arizona Department of Water Resources web site, accessed on March 15, 2018, at http://www.azwater.gov/AzDWR/StatewidePlanning/WaterAtlas/CentralHighlands/PlanningAreaOverview/WaterSupply-Groundwater.htm.

Arizona Department of Water Resources, 2014c, Active management area water supply—groundwater: Arizona Department of Water Resources web site, accessed on March 20, 2018, at http://www.azwater.gov/azdwr/StatewidePlanning/WaterAtlas/ActiveManagementAreas/PlanningAreaOverview/WaterSupplyGroundwater.htm.

Arizona Department of Water Resources, 2014d, Groundwater hydrology in the Verde River Basin: Arizona Department of Water Resources web site, accessed November 2018 at http://www.azwater.gov/AzDWR/StatewidePlanning/WaterAtlas/CentralHighlands/Hydrology/VerdeRiver.htm.

Arizona State Legislature, 1980, Groundwater code: Arizona State Legislature revised statutes, title 45, chapter 2, accessed August, 19 2018, at https://www.azleg.gov/arsDetail/?title=45.

Barnes, W.C., 1988, Arizona place names: Tucson, Arizona, The University of Arizona Press, 504 p.

Bilodeau, W.L., 1986, The Mesozoic Mogollon highlands, Arizona—an early Cretaceous rift shoulder: Geology, v. 94, p. 724–735.

Blakey, R.C., 1990, Stratigraphy and geologic history of Pennsylvanian and Permian rocks, Mogollon Rim region, central Arizona and vicinity: Geological Society of America Bulletin, v. 102, p. 1189–1217.

Blasch, K.W., Hoffman, J.P., Graser, L.F., Bryson, J.R., and Flint, A.L., 2006, Hydrogeology of the upper and middle Verde River watersheds, central Arizona: U.S. Geological Survey Scientific Investigations Report 2005–5198, 101 p., 3 plates.

Collins, T.W., and Bolin, R., 2007, Characterizing vulnerability to water scarcity—The case of a groundwater-dependent, rapidly urbanizing region: Environmental Hazards, v. 7, p. 399–418.

Coney, P.J., and Reynolds, S.J., 1977, Cordilleran Benioff zones: Nature, v. 270, p. 403–406.

Cooley, M.E., and Davidson, E.S., 1963, The Mogollon Highlands—their influence on Mesozoic and Cenozoic erosion and sedimentation: Arizona Geological Society Digest, v. 6, p. 7–35.

Corkhill, E.F., and Mason, D.A., 1995, Hydrogeology and simulation of groundwater flow, Prescott Active Management Area, Yavapai County, Arizona: Arizona Department of Water Resources Modeling Report 9, 143 p., 3 sheets, scales 1:170,000 and 1:300,000.

Dater, D., Metzger, D., and Hittelman, A., comps., 1999, Land and marine gravity CD-ROMS: Boulder, Colorado, National Geophysical Center.

Davis, G.H., 1978, Monocline fold pattern of the Colorado Plateau, in Matthews, V., III, ed., Laramide folding associated with basement block faulting in the Western United States: Geological Society of America Memoir 151, p. 215–233.

DeWitt, E., Langenheim, V., Force, E., Vance, R.K., Lindberg, P.A., and Driscoll, R.L., 2008, Geologic map of the Prescott National Forest and the headwaters of the Verde River, Yavapai and Coconino Counties, Arizona: U.S. Geological Survey Scientific Investigations Map 2996, 100 p., 1 sheet, scale 1:100,000.

DeWitt, E., Langenheim, V.E., and Wirt, L., 2005, Geologic framework in Wirt, L., DeWitt, E., and Langenheim, V.E., eds., Geologic framework of aquifer units and ground-water flowpaths, Verde River headwaters, north-central Arizona: U.S. Geological Survey Open-File Report 2004–1411-B, 28 p.

Dixon, J.M., and Farrar, E., 1980, Ridge subduction, eduction, and the Neogene tectonics of southwestern North America: Tectonophysics, v. 67. p. 81–99.

Elston, D.P., and Young, R.A., 1991, Cretaceous-Eocene (Laramide) landscape development and Oligocene-Pliocene drainage reorganization of transition zone and Colorado Plateau, Arizona: Journal of Geophysical Research, v. 96, no. B7, p. 12,389–12,406.

Ewing, D.B., Osterberg, J.C., and Talbot, W.R., 1994a, Ground water study of the Big Chino Valley section I of III, Perspective: Denver, Colorado, Bureau of Reclamation technical report, 8 p.

Ewing, D.B., Osterberg, J.C., and Talbot, W.R., 1994b, Ground water study of the Big Chino Valley, section III of III, Hydrology and hydrogeology: Denver, Colorado, Bureau of Reclamation technical report, 18 p.

Frank, A.J., 1984, Analysis of gravity data from the Picacho Butte area, Yavapai and Coconino counties, Arizona: Flagstaff, Arizona, Northern Arizona University M.S. thesis, 91 p.

Freethey, G.W., and Anderson, T.W., 1986, Predevelopment hydrologic conditions in the alluvial basins of Arizona and adjacent parts of California and New Mexico: U.S. Geological Survey Hydrologic Atlas 664, 3 plates.

Garner, B.D., and Bills, D.J., 2012, Spatial and seasonal variability of base flow in the Verde Valley, central Arizona, 2007 and 2011: U.S. Geological Survey Scientific Investigations Report 2012–5192, 33 p.

Graham, P.J., 2007, Sustaining people, habitats, and ecosystems—The challenge of integrating water policy and the environment, chap. 7 of Colby, B.G., and Jacobs, K.L., eds., Arizona water policy—Management innovations in an urbanizing, arid region: New York, Routledge, p. 92–105.

Harshbarger, J.W., Repenning, C.A., and Irwin, J.H., 1957, Stratigraphy of the uppermost Triassic and the Jurassic rocks of the Navajo country, U.S. Geological Survey Professional Paper 291, 74 p.

Langenheim, V.E., Duval, J.S., Wirt, Laurie, and DeWitt, Ed, 2000, Preliminary report on geophysics of the Verde River headwaters region, Arizona: U.S. Geological Survey Open-File Report 00-403, 28 p. (https://pubs.usgs.gov/of/2000/0403/).

Langenheim, V.E., Hoffmann, J.P., Blasch, K.W., Dewitt, E., and Wirt, L., 2002, Preliminary report on geophysical data in Yavapai County, Arizona: U.S. Geological Survey Open-File Report 02-352, 29 p.

Langenheim, V.E., DeWitt, E., and Wirt, L., 2005, Geophysical framework based on analysis of aeromagnetic and gravity data, Verde River headwaters, north-central Arizona, in Wirt, L., DeWitt, E., and Langenheim, V.E., eds., Geologic framework of aquifer units and ground-water flowpaths in the Verde River Headwaters: U.S. Geological Survey Open-File Report 04–1411, p. C1-C26.

Macy, J.P., and Heilman, J.A., 2018, Controlled source audio-frequency magnetotellurics (CSAMT) data from the Big Chino Wash and Paulden areas, Yavapai County, Arizona: U.S. Geological Survey data release, https://doi.org/10.5066/P9KGKWNL.

Marder, M.K., 2009, The battle to save the Verde—How Arizona's water law could destroy one of its last free-flowing rivers: Arizona Law Review, v. 51, p. 175–210.

McKee, E.D., 1937, Triassic pebbles in northern Arizona containing invertebrate fossils: American Journal of Science, v. 33, p. 260–263.

Middleton, L.T., and Elliott, D.K., 2003, Tonto group, *in* Beus, S.S., and Morales, M., eds., Grand Canyon Geology: New York, Oxford University Press, p. 90–106.

Montgomery, E.L., and Harshbarger, J.W., 1989, Arizona hydrogeology and water supply, in Jenney, J.P. and Reynolds, S.J., eds., Geologic evolution of Arizona: Arizona Geological Society Digest, v. 17, p. 827–840.

Munoz-Erickson, T.A., Cutts, B.B., Larson, E.K., Darby, K.J., Neff, M., Wutich, A., and Bolin, R., 2010, Spanning boundaries in an Arizona watershed partnership—Information networks as tools for entrenchment or ties for collaboration?: Ecology and Society, v. 15, no. 3, 22 p.

Nabighian, M.N., and Macnae, J.C., 1991, Time domain electromagnetic prospecting methods in Nabighian, M.N., ed., Electromagnetic methods in applied geophysics, volume II: Tulsa, Okla., Society of Exploration Geophysicists, p. 427–520.

Navarro, L.F., 2002, Characterization and groundwater flow modeling of the Mint Wash/Williamson Valley area, Yavapai County: Flagstaff, Ariz., Northern Arizona University, M.S. thesis, 158 p.

Owen-Joyce, S.J., and Bell, C.K., 1983, Appraisal of water resources in the upper Verde River area, Yavapai and Coconino Counties, Arizona: Arizona Department of Water Resources Bulletin 2, 219 p.

Ostenaa, D.A., Schmischal, U., King, C.E., Jr., and Wright, J.W., 1993, Ground water study of the Big Chino Valley, section II of III, Geologic framework investigations: Denver, Colorado, Bureau of Reclamation v. 1, 31 p., 9 plates.

Palacky, G.J., 1991, Resistivity characteristics of geologic targets, in Nabighian, M.N., ed., ., Electromagnetic methods in applied geophysics, volume II: Tulsa, Okla., Society of Exploration Geophysicists, p. 53–129.

Pierce, H.W., Damon, P.E., and Shafiqullah, M., 1979, An Oligocene (?) Colorado Plateau edge in Arizona: Tectonophysics, v. 61, p. l–24.

Pool, D.R., Blasch, K.W., Callegary, J.B., Leake, S.A., and Graser, L.F., 2011, Regional groundwater-flow model of the Redwall-Muav, Coconino, and alluvial basin aquifer systems of northern and central Arizona: U.S. Geological Survey Scientific Investigations Report 2010–5180, v. 1.1, 101 p.

Rothman, D.W. and Mays, L.W., 2014, Water resources sustainability—Development of a multi-objective optimization model: Journal of Water Resources Planning and Management, v. 140, no. 12, 9 p.

Schwab, K.J., 1995, Maps showing groundwater conditions in the Big Chino Sub-basin of the Verde River Basin, Coconino and Yavapai Counties, Arizona—1992: Arizona Department of Water Resources Hydrologic Map Series Report no. 28, 2 sheets, scale 1:250,000.

Sharma, P.V., 1997, Environmental and engineering geophysics: Cambridge, U.K., Cambridge University Press, 475 p.

Simpson, F., and Bahr, K., 2005, Practical magnetotellurics: Cambridge, U.K., Cambridge University Press, 254 p.

Sine, C.R., Wilson, D., Gao, W., Grand, S.P., Aster, R., Ni, J., and Baldridge, W.S., 2008, Mantle structure beneath the western edge of the Colorado Plateau: Geophysical Research Letters, v. 35, L10303.

Spencer, J.E., and Reynolds, S.J., 1989, Middle Tertiary tectonics of Arizona and adjacent areas, in Jenney, J.P., and Reynolds, S.J., eds., Geologic evolution of Arizona: Arizona Geological Society Digest, v. 17, p. 539–574.

U.S. Census Bureau, 2018, American FactFinder: U.S. Census Bureau web site, accessed September, 2018, https://factfinder.census.gov/faces/nav/jsf/pages/community_facts.xhtml.

U.S. Geological Survey, 1979, Water resources data for Arizona, water year 1978: U.S. Geological Survey Water-Data Report AZ-78-1, 604 p.

U.S. Geological Survey, 1980, Water resources data for Arizona, water year 1979: U.S. Geological Survey Water-Data Report AZ-79-1, 614 p.

U.S. Geological Survey and Arizona Geological Survey, 2018, Quaternary fault and fold database for the United States: U.S. Geological Survey website, accessed November 2018 at http://earthquake.usgs.gov/hazards/qfaults/.

van Wijk, J.W., Baldridge, W.S., van Hunen, J., Goes, S., Aster, R., Coblentz, D.D., Grand, S.P., and Ni, J., 2010, Small-scale convection at the edge of the Colorado Plateau—Implications for topography, magmatism, and evolution of Proterozoic lithosphere: Geology, v. 38, no. 7, p. 611–614.

Wallace, B.L., and Laney, R.L., 1976, Maps showing groundwater conditions in the lower Big Chino Valley and Williamson Valley areas, Yavapai and Coconino Counties, Arizona—1975–76: U.S. Geological Survey Water-Resources Investigations Report 76-78, 2 sheets, scale 1:125,000.

Water Resources Associates, Inc., 1989, Hydrogeology investigation, Big Chino Valley, Yavapai county, Arizona, Phase I: City of Prescott, Arizona, City Attorney's Office, 2 volumes.

Wilson, R.P., 1988, Water resources of the northern part of the Agua Fria area, Yavapai County, Arizona: Arizona Department of Water Resources Bulletin 5, 109 p.

Wilson, R.P., 1991, Summary of ground-water conditions in Arizona, 1985–86: U.S. Geological Survey Water-Resources Investigations Report 90–4179, 4 sheets, various scales.

Wirt, L., DeWitt, E., and Langenheim, V.E., 2005, Geologic framework of aquifer units and ground-water flowpaths, Verde River headwaters, north-central Arizona: U.S. Geological Survey Open-File Report 2004–1411.

Wirt, L., and Hjalmarson, H.W., 2000, Sources of springs supplying base flow to the Verde River headwaters, Yavapai County, Arizona: U.S. Geological Survey Open-File Report 99–0378, 50 p.

Wirt, F.N., DeWitt, E., and Langenheim, V.E., 2005, Hydrogeologic framework in Wirt, L., DeWitt, E., and Langenheim, V.E., eds., Geologic framework of aquifer units and groundwater flowpaths, Verde River headwaters, north-central Arizona: U.S. Geological Survey Open-File Report 2004-1411-D, 27 p.

Yavapai-Apache Nation, 2018, Welcome to the Yavapai-Apache Nation Gah'nahvah: To Tell (Yavapai) | Ya Ti: To Talk (Apache): Yavapai-Apache Nation web site, accessed September 2018 at http://www.yavapai-apache.org/.

Yungul, S.H., 1996, Electrical Methods in Geophysical Exploration of Deep Sedimentary Basins: New York, Chapman and Hall, 208 p.

Zohdy, A.A.R., Eaton, G.P., and Mabey, D.R., 1974, Application of surface geophysics to ground-water investigations: U.S. Geological Survey Techniques of Water-Resources Investigations, book 2, chap. D1, 116 p.

Zonge, K., 1992, Broadband electromagnetic systems, in Van Blaricom, R., ed., Practical geophysics II for the exploration geologist: Spokane, Wash., Northwest Mining Association, 96 p.

Publishing support provided by the Menlo Park Publishing Service Center, California
Manuscript approved for publication August 7, 2019
Edited by Claire Landowski
Cartography and graphic design by JoJo Mangano
Layout by Kimber Petersen

ISSN 2330-7102 (online)
https://doi.org/10.3133/sir2015082